communications biology

A Nature Portfolio journal

Article

https://doi.org/10.1038/s42003-025-07823-4

Metabolic crosstalk between the mitochondrion and the nucleus is essential for *Toxoplasma gondii* infection

Check for updates

Hongxi Zhang[1,6], Nuo Ji[1,6], Shuxin Su[2,6], Meng Zhao[1], Huiyu Du[1], Lakesh Kumar Sahoo[3], Yi Wu[2], Yaoyu Feng[1,4], Nishith Gupta[3,5] ✉, Lihua Xiao[1,4] ✉ & Ningbo Xia[1,4] ✉

Toxoplasma gondii, an intracellular pathogenic protist with a remarkable ability to infect a wide range of host cells, displays an equally exceptional design of its carbon metabolism. There are, however, critical gaps in our understanding of the metabolic network in *T. gondii*. We characterized the mito-nuclear metabolism and organelle coupling during its acute infection (lytic cycle). The major enzymes of the TCA cycle, i.e., citrate synthase (CS1), succinyl-CoA synthase alpha subunit (SCSα), succinate dehydrogenase (SDHA) and FAD malate dehydrogenase (MDH-FAD) located in the parasite mitochondrion support its asexual reproduction but are not needed for its survival. The SCSα and SDHA mutants are nearly avirulent in a mouse model, and they can protect the host against a lethal challenge infection. Genetic deletion of MDH-FAD dysregulated glucose-derived carbon flux, leading to a collapse of the mitochondrial membrane potential. The parasite also harbors a cytosolic isoform of MDH and a nuclear malic enzyme (ME) contributing to malate oxidation; however, only the latter is essential for the lytic cycle. Expression of ME in the nucleus is crucial for the parasite development. Besides, conditional knockdown of ME impairs the histone acetylation and disrupts the expression of several genes in tachyzoites. Our work discloses novel network design features of *T. gondii* and highlights the therapeutic and vaccination potential of the parasite metabolism.

T oxoplasma gondii, a prevalent zoonotic parasite, infects many warm-blood organisms and can reproduce in several nucleated host cells[1]. It has a complex life cycle, with sexual reproduction occurring exclusively in felid hosts and asexual development in a wide range of intermediate hosts, such as pigs, cattle, sheep and humans[1]. The parasite exists in two infectious stages in its hosts: fast-replicating tachyzoites and slow-growing bradyzoites. Acute toxoplasmosis in pregnant individuals or animals can cause abortion, stillbirth or fetal deformities[1]. In contrast, the chronic disease usually persists for the entire life of the infected host and can result in recrudescence upon impairment of the immunity. These outcomes seriously threaten public health and socioeconomic development. Currently, pyrimethamine and sulfadiazine are the only common drugs for treating acute toxoplasmosis[2–4] and none are available for against chronic infection. Extended drug usage is also associated with adverse effects and drug resistance[2–4]. There is only one commercial vaccine (Toxovax), which is weakly virulent and used exclusively in sheep, with a potential risk of reverting to virulence. Therefore, there is an urgent need to explore additional drug and vaccine targets to control the disease[5,6]. Although the parasite metabolism remains central to drug development, its limited knowledge has hindered the discovery of new therapeutic vulnerabilities in *T. gondii*.

Toxoplasma's acutely infectious tachyzoite stage utilizes glucose- and glutamine-derived carbon to fuel their carbon metabolism and, thereby, the lytic cycle[7–11]. Glucose and glutamine are metabolized through glycolysis and the TCA cycle, respectively, and both nutrients cooperate to enable a

[1]State Key Laboratory for Animal Disease Control and Prevention, South China Agricultural University, Guangzhou, China. [2]Frontiers Science Center for Synthetic Biology and Key Laboratory of Systems Bioengineering (Ministry of Education), School of Chemical Engineering and Technology, Tianjin University, Tianjin, China. [3]Intracellular Parasite Education And Research Labs (iPEARL), Department of Biological Sciences, Birla Institute of Technology and Science, Pilani (BITS Pilani), Hyderabad, India. [4]Guangdong Laboratory for Lingnan Modern Agriculture, Center for Emerging and Zoonotic Diseases, College of Veterinary Medicine, South China Agricultural University, Guangzhou, China. [5]Department of Molecular Parasitology, Institute of Biology, Faculty of Life Sciences, Humboldt University, Berlin, Germany. [6]These authors contributed equally: Hongxi Zhang, Nuo Ji, Shuxin Su. ✉e-mail: Gupta.Nishith@hyderabad.bits-pilani.ac.in; lxiao@scau.edu.cn; ningboxia@scau.edu.cn

rapid propagation of tachyzoites. Glucose enters the parasite through a high-affinity transporter located in the plasma membrane[7] and then converted to pyruvate *via* glycolysis[8,10,12]. Pyruvate is imported into the mitochondrion *via* the mitochondrial pyruvate carrier (MPC) complex, where it is converted to acetyl-coenzyme A (Ac-CoA) by a branched-chain α-ketoacid dehydrogenase E1 subunit (BCKDH-E1α), feeding into the TCA cycle[13,14]. However, tachyzoite mutants lacking MPC or BCKDH-E1α are still viable and partially virulent[13,14]. Glutamine is first converted to glutamate, entering the TCA cycle as α-ketoglutarate or as succinate *via* a γ-aminobutyric acid (GABA) shunt[8]. Tachyzoites can also survive the deletion of glutamate decarboxylase (GAD), the first enzyme of the GABA shunt, although their growth and virulence are impaired[8]. These studies reveal significant vulnerabilities and plasticity in the parasite metabolism. The TCA cycle is a vital eukaryotic pathway, but its significance for the asexual growth of *T. gondii* remained ambiguous. The tachyzoite stage harbors all enzymes expressed in the mitochondrion[15], and stable isotopic labeling showed evidence of a canonical oxidative-type TCA cycle[8]. The first step is catalyzed by citrate synthase 1 (CS1), forming citrate from acetyl-CoA and oxaloacetate. Subsequently, aconitase (ACO) isomerizes citrate to isocitrate, which is then oxidized to α-ketoglutarate by isocitrate dehydrogenase I (IDH1). α-ketoglutarate serves as a substrate for α-ketoglutarate dehydrogenase (KDH), producing succinyl-CoA, which is converted to succinate by succinyl-CoA-synthetase (SCS). Depletion of the SCSα subunit only partially (~30% reduction) impairs parasite growth, suggesting an alternative pathway for succinate production[15]. A succinic semialdehyde dehydrogenase (SSADH) is also present in the parasite genome, which can potentially produce succinate from succinic semialdehyde[16]. The latter may originate from γ-aminobutyric acid (GABA) shunt in tachyzoites[8]. However, the physiological role of SSADH in *T. gondii* remains unknown.

Succinate is oxidized by succinate dehydrogenase (SDH) to form fumarate, which in turn is hydrated to produce malate by the catalytic action of fumarate hydratase (FH). Malate is oxidized to oxaloacetate by malate dehydrogenase (MDH). Oxaloacetate has multiple fates depending on the physiological status of the parasite. It can fuse with acetyl-CoA, completing the TCA cycle[8], and is used for aspartate synthesis *via* aspartate aminotransferase/glutamic oxaloacetic transaminase (AST/GOT)[10]. Additionally, during gluconeogenesis in glucose-starved conditions, oxaloacetate drives the formation of phosphoenolpyruvate by a mitochondrial isoform of phosphoenolpyruvate kinase (PEPCK)[11]. The latter two are cataplerotic reactions, which dispose of TCA cycle intermediates to other pathways. Glutamate dehydrogenase (GDH) catalyzing the formation of glutamate from α-ketoglutarate and the malic enzyme (ME) producing pyruvate from malate are other cataplerotic proteins encoded by the parasite, but their physiological relevance has not been studied. The parasite also harbors two variants of malate dehydrogenases: MDH and MDH-FAD[15]; however, neither has been examined in *T. gondii*.

The cataplerotic contribution of the TCA cycle to biosynthetic pathways necessitates anaplerotic replenishment of its intermediates to ensure continued operation. Pyruvate carboxylase (PyC), which converts pyruvate to oxaloacetate in the mitochondrial matrix, is the typical anaplerotic enzyme and is also present in *T. gondii*. However, it is dispensable in both glycolysis-competent and glycolysis-deficient tachyzoites[11]. Hence, its metabolic role remains unknown. This study presents a systematic dissection of the central carbon metabolism in *T. gondii* by genetic mutagenesis of CS1, SSADH, SCSα, SDHA, ME, MDH-FAD and MDH. In-depth phenotyping of the mutants coupled with metabolomics discloses novel design features and therapeutic targets in the core metabolic network of *T. gondii*.

Results

The CS1 is needed for the growth but not for the survival of tachyzoites

The genome of *T. gondii* harbors three isoforms of citrate synthase (www.ToxoDB.org); however, only CS1 is located in the tachyzoite mitochondrion[15]. We started our work confirming the subcellular location of CS1 in the mitochondrion by 3'-genomic tagging (Fig. 1a). The *CS1*-specific CRISPR/Cas9 construct and the homology donor amplicon encoding YFP-*DHFR** were transfected into tachyzoites to generate a *Δcs1* mutant (YFP$^+$) (Supplementary Fig. 1a). Surprisingly, we could isolate a *CS1* deletion strain despite its predicted essentiality in tachyzoites[17,18]. Genomic PCR screening (Supplementary Fig. 1b), genome sequencing (Supplementary Fig. 4a), and indirect immunofluorescence assays (IFA) confirmed the deletion of the *CS1* locus in the mutant (Supplementary Fig. 1c). The *Δcs1* mutant grew slower in routine culture and produced smaller plaques due to poor replication than the parental strain (Fig. 1b–d). The *Δcs1* mutant was severely attenuated in mice as judged by their higher survival rate at doses of 10^2 parasites/mouse (84%, Fig. 1e). Even at higher doses (up to 10^4 parasites/mouse), 84% of animals survived the infection (Fig. 1e). The parasite load in mutant-infected animals was almost 10^4 times lower than the parental (*DiCre*) strain (Fig. 1f). These results reveal that CS1 is required for optimal growth and virulence but is not essential for tachyzoite survival.

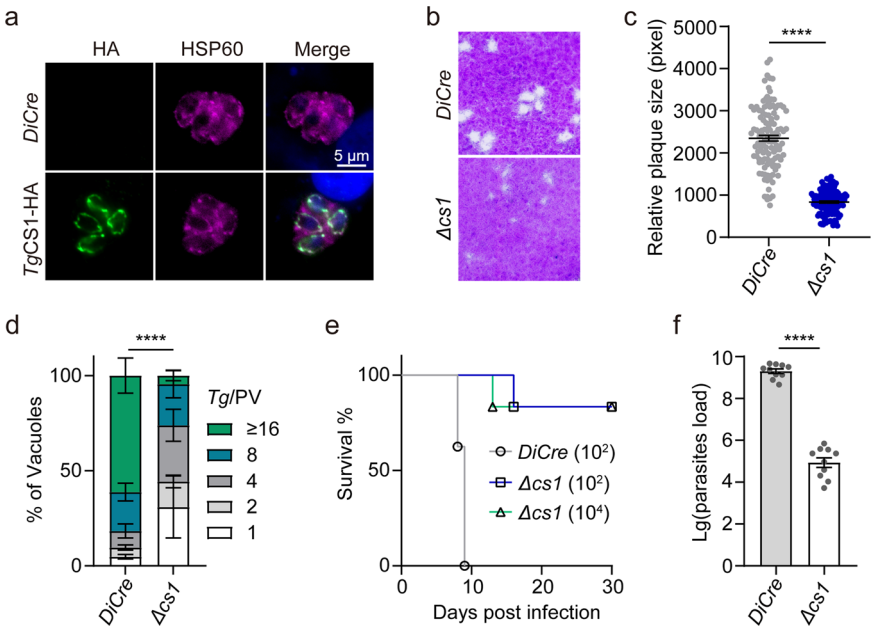

Fig. 1 | CS1 is required for parasite growth. **a** CRISPR/Cas9-assisted 3'-genomic tagging of the CS1 gene with a spaghetti monster HA (smHA) tag in the RH*Δku80* strain. HSP60 (magenta) was used as a mitochondrial marker. Scale bars, 5 μm. **b** A 7-day plaque assay to evaluate the growth of *DiCre* (RH DiCre_T2A *Δku80Δhxgprt*) and *Δcs1* mutant (100 tachyzoites/well, 3 wells/strain). **c** The relative size of plaques from (**b**) (means ± SEM; ****$p \le 0.0001$, Student's *t* test). **d** Replication efficiency of *DiCre* and *Δcs1* strains. The number of vacuoles was counted 24 hours post-invasion ($n = 4$ independent experiments, means ± SEM; two-way ANOVA). **e** Virulence test of ICR mice infected with *DiCre* or *Δcs1* stains (10^2 or 10^4 parasites/mouse and 6–8 mice/group). **f** Parasite burden in the peritoneal fluid of mice. ICR mice were infected with *DiCre* or *Δcs1* mutants (10^4 tachyzoites/mouse and 5 mice/strain). Parasite load in peritoneal fluid was calculated 5 days post-infection by qPCR based on the non-coding fragment length of 529 bp.

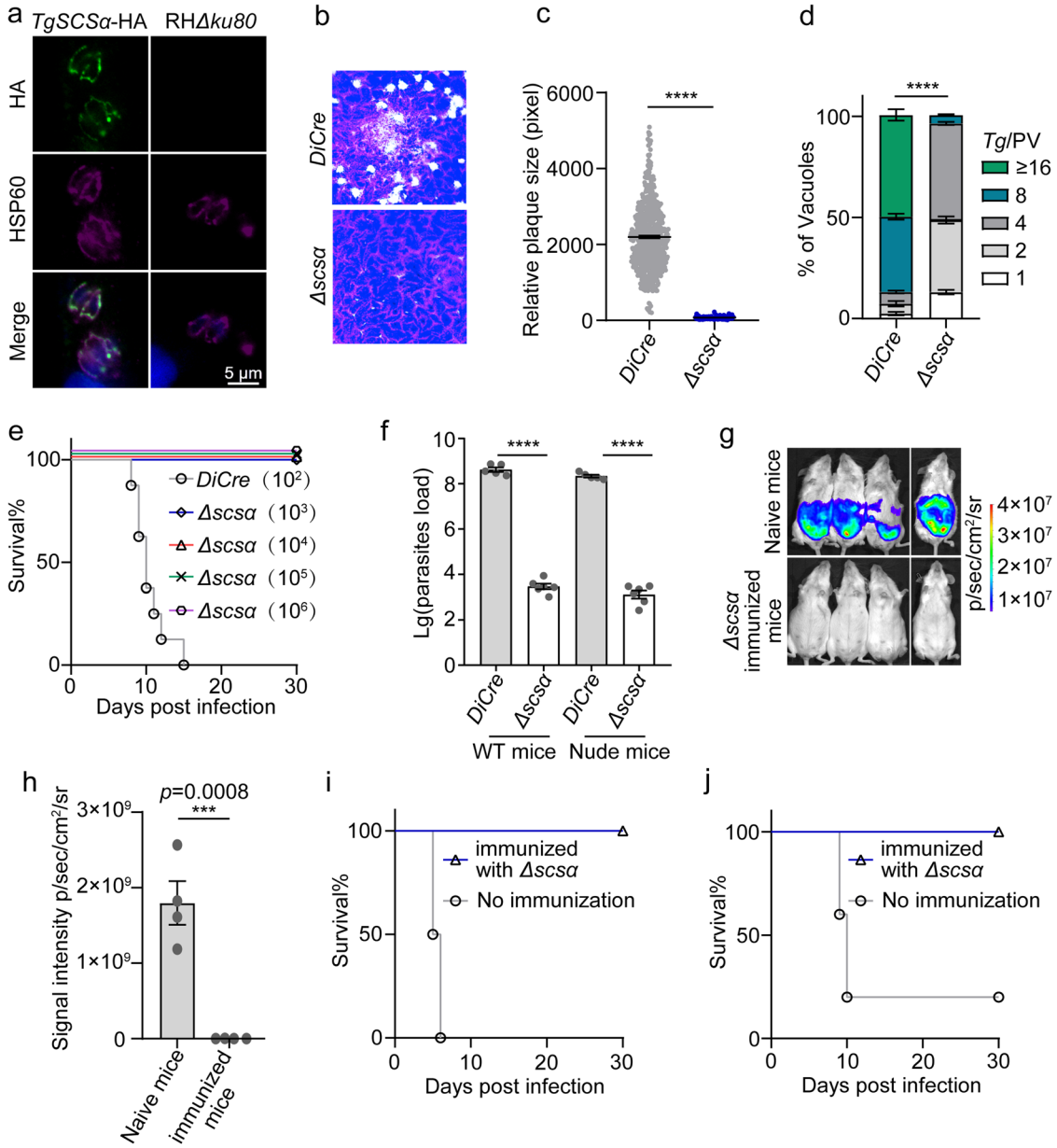

Fig. 2 | SCSα is vital for the lytic cycle of *T. gondii*. **a** Endogenous tagging of SCSα confirms its mitochondrial localization. **b** A 7-day plaque assay to assess the growth of *DiCre* and *Δscsα* strains (100 tachyzoites/well and 3 wells for each strain). **c** The relative size of plaques from (**b**) (means ± SEM; ****$p \le 0.0001$, Student's *t* test). **d** Intracellular growth of *Δscsα* in vitro. The strain was cultured for 24 h after infection with HFF cells, and the number of parasites in vacuoles was recorded by IFA ($n = 3$ independent experiments, means ± SEM; two-way ANOVA). **e** Virulence tests of *DiCre* and *Δscsα* strains in ICR mice (10^2, 10^3, 10^4, 10^5, 10^6 parasites/mouse and 5–8 mice/group). **f** ICR mice (WT) or immunodeficient mice (BLAB/c nude) infected with *DiCre* and *Δscsα* strains (10^4 tachyzoites/mouse, 5–6 mice/strain). 5 days after infection, the parasite load in the peritoneal fluid was analyzed by qPCR. (means ± SEM; *t*-test). **g** Naive or *Δscsα*-immunized mice were infected with 10^4 RH-*Luc* tachyzoites (4 mice in each group). The parasite load of mice was analyzed by the IVIS Spectrum imaging system 5 days after RH-*Luc* infection. **h** The bioluminescence signal intensity of mice from (**g**) was calculated and plotted. **i** The survival of naive or *Δscsα* immunized mice infected with RH-*Luc* (**$p = 0.0084$, simple survival analysis). **j** The survival of naive or *Δscsα*-immunized mice infected with 10^4 ME49 tachyzoites. Statistical significance was examined by log-rank Mantel–Cox test (*$p = 0.0144$).

Deletion of *SCSα* compromises parasite growth, whereas SSADH is dispensable

To gain additional insight into the importance of the TCA cycle, we investigated SCSα. The HA-tagged SCSα is also expressed in the mitochondrion (Fig. 2a). Earlier work has shown that ATc-mediated depletion of *SCSα* transcript inflicts only minor growth defects in tachyzoites[15]. Such an unexpected (poor) phenotype upon conditional knockdown can be attributed to a lack of stringent regulation by ATc or a nonessential role of SCSα. We, therefore, engineered a *SCSα* deletion mutant by CRISPR/Cas9-assisted homologous gene replacement (Supplementary Fig. 1f). The *Δscsα* (YFP^+) mutant was isolated after pyrimethamine selection, diagnostic PCR screening and immunostaining (Supplementary Fig. 1g, h). The *Δscsα* strain was notably viable in prolonged culture despite severely impaired plaque formation and replication defect (Fig. 2b–d). The data indicate a partial TCA cycle operation is sufficient for parasite survival.

We also investigated SSADH, which can produce succinate from succinic semialdehyde[16]. The 3'HA-tagged SSADH was expressed in the mitochondrion, co-localizing with HSP60 – a known organelle marker (Fig. 3a). We next engineered a *Δssadh* strain using CRISPR/Cas9-mediated homologous recombination (Supplementary Fig. 1d), pyrimethamine

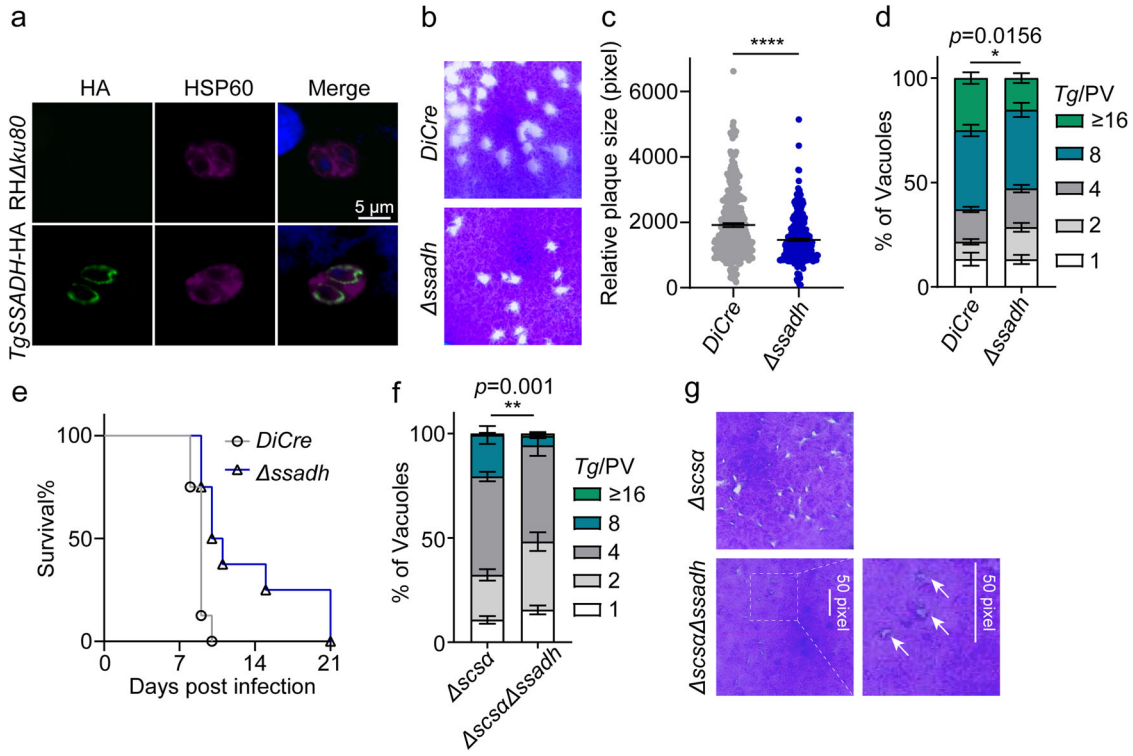

Fig. 3 | *SSADH* deletion only mildly affects parasite development. a SSADH was localized in the mitochondria of *T. gondii*, co-localized with the mitochondrial marker protein HSP60. **b** A 7-day plaque assay using the *DiCre* and *Δssadh* strain (100 tachyzoites/well, 3 wells/strain). **c** The relative size of plaques from panel (**b**). **d** The replication of *Δssadh*. The number of parasites in the vacuole was recorded after 24 h of culture in HFF cells (mean ± SEM; two-way ANOVA). **e** Virulence test of ICR mice infected with *DiCre* and *Δssadh* parasites (100 tachyzoites/mouse and 8 mice/strain). **f** Replication efficiency of the *Δscsα* and *ΔscsαΔssadh* strains. The number of vacuoles was counted 24 h post-infection. **g** A 10-day plaque assay of the *Δscsα* and *ΔscsαΔssadh* strains (100 tachyzoites/well, 3 wells/strain).

selection and PCR screening (Supplementary Fig. 1e). The gene deletion had only a minor impact on plaque formation (Fig. 3b, c), replication (Fig. 3d) and virulence (Fig. 3e), ruling out SSADH as a primary source for succinate entry into the TCA cycle. Functional redundancy of SSADH and SCSα was examined by deleting *SSADH* in the *Δscsα* strain, resulting in a double mutant (*ΔscsαΔssadh*) (Supplementary Fig. 2a–c). Phenotyping revealed a further reduction in the replication of *ΔscsαΔssadh* (Fig. 3f); however, the mutant could be maintained in cultures (Fig. 3g). This finding consolidates our other data on the metabolic flexibility in the TCA cycle.

The *Δscsα* mutant is avirulent, and it can protect mice from challenge infection

Our further work evaluated the in vivo relevance of the *Δscsα* strain by intraperitoneal injection into the ICR mice. As expected, the parental (*DiCre*) strain killed almost all animals within 2 weeks (Fig. 2e). In contrast, mice infected with *Δscsα* survived and exhibited no clinical signs. Even at much higher doses of the mutant (~10^6 tachyzoites/mouse), no apparent virulence was observed (Fig. 2e). The *Δscsα* and *DiCre* strains (10^4 tachyzoites/animal) were also quantified in the peritoneal fluid by qPCR five days post-infection. The parasite burden in mice parasitized by the mutant was at or below the detection threshold of qPCR (Fig. 2f). We tested whether the host immune response underpins the attenuated growth of the *Δscsα* strain in mice. Immunodeficient Balb/c-nu mice were infected (10^4 parasites/animal), and the parasite load was quantified. The outcome resonated with the immune-competent ICR mice, as the *Δscsα* tachyzoites were barely detectable in the Balb/c-nu mice (Fig. 2f).

In the next step, we explored the potential of genetically attenuated *Δscsα* strain as a whole-cell vaccine because it could be cultured in vitro but failed to proliferate in vivo. Indeed, the *Δscsα*-immunized mice rapidly cleared the challenge infection by the RH-*Luc* tachyzoites, as evident by bioimaging of luminescence (Fig. 2g, h). Furthermore, all *Δscsα*-vaccinated animals survived infection of RH-*Luc* and ME49 tachyzoites (Fig. 2i, j). In conclusion, our data highlight the therapeutic and vaccination potential of SCSα protein and *Δscsα* mutant, respectively. The inability of the *Δscsα* strain to propagate itself in mice also suggests a critical in vivo role of SCSα in the mitochondrial metabolism.

SDHA and FH are vital, but MDH and OMT are dispensable in tachyzoites

In the next step, succinate is oxidized to fumarate by SDH, also known as complex II, because it delivers TCA cycle-derived electrons to the mitochondrial electron transport chain (mETC)[19]. *Toxoplasma* SDH is a large complex of over 500 kDa, broadly divided into a membrane-anchoring domain and an enzymatic core. The latter, localizing in the matrix, comprises SDHB and SDHA. The SDHA contains the succinate-binding site and the FAD cofactor[19]. We generated an *SDHA* mutant confirmed by PCR screening and immunostaining (Supplementary Fig. 1i–k). The *Δsdha* was severely compromised compared to the parental strain (Fig. 4a–c). Accordingly, the mutant could not propagate in vivo (Fig. 4d), resulting in the survival of all infected mice (Fig. 4e). Even at much higher doses of the *Δsdha* mutant (~10^5 tachyzoites/mouse), no significant virulence was observed (Fig. 4f). Similar to the *Δscsα* mutant, immunization of mice with *Δsdha* induced effective host immune protection against challenge with wild-type RH-*Luc* and ME49 (Fig. 4g–j). Next, we tried to ablate the fumarate hydratase (FH) protein, converting SDHA-derived fumarate to malate. However, our efforts to delete the *FH* gene were unsuccessful, suggesting its necessity for parasite survival.

Our following work focused on MDH, oxidizing malate into oxaloacetate. It was earlier shown to localize on the parasite mitochondrion[15]. However, 3'-genomic tagging of MDH with an HA tag revealed its expression in the cytoplasm, localizing with ALD (Fig. 5a). To assess its physiological importance, we engineered a knockout strain using the CRISPR/Cas9 system (Supplementary Fig. 3a). PCR screening (Supplementary Fig. 3b) and genome sequencing (Supplementary Fig. 4b) verified

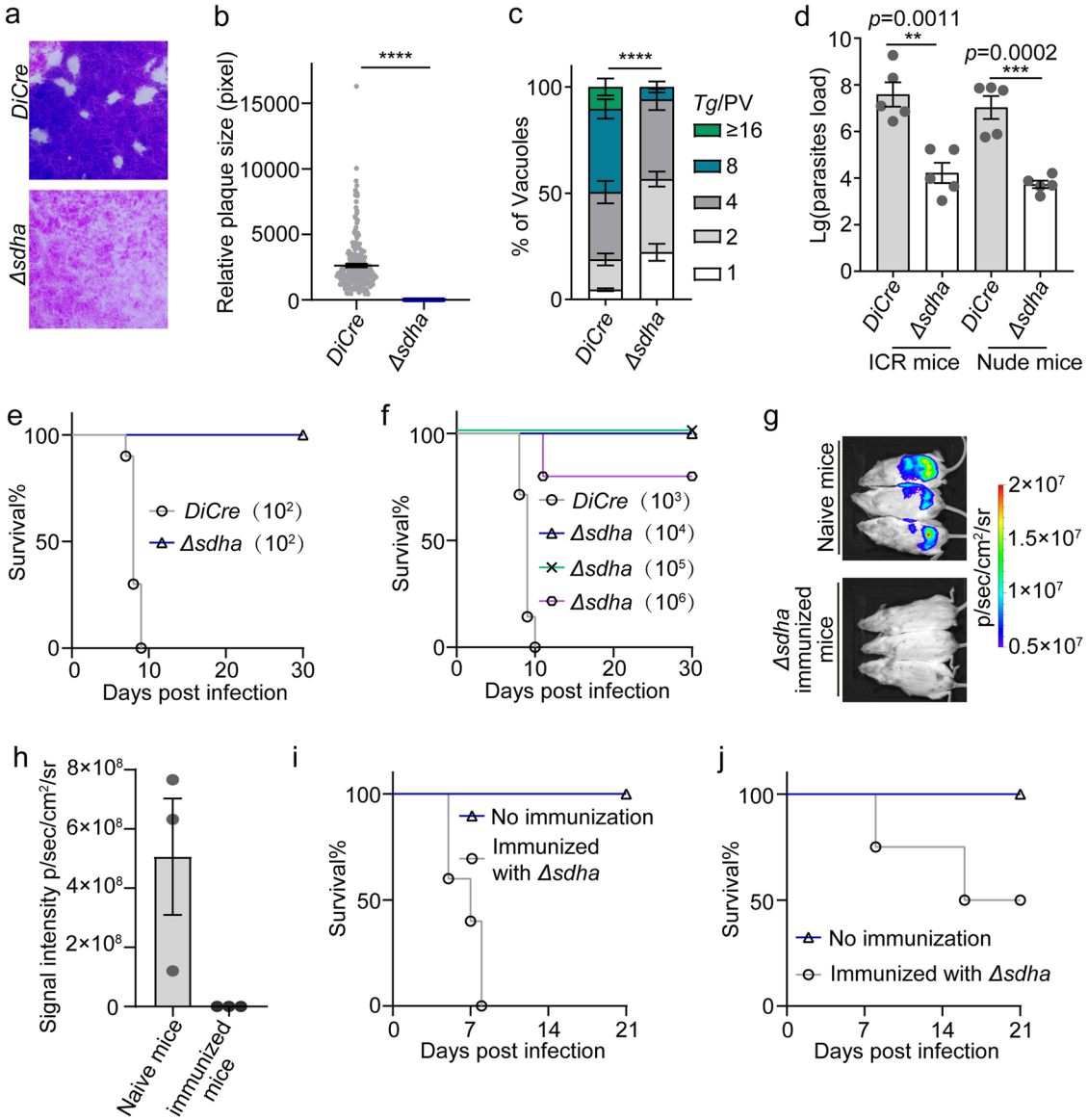

Fig. 4 | Knockout of *SDHA* is detrimental for the parasite. a A 6-day plaque assay to assess the growth of *DiCre* and *Δsdha* strains (100 tachyzoites/well and 3 wells for each strain). **b** The relative size of the plaques from (**a**). **c** The replication efficiency of *DiCre* and *Δsdha* strains in HFF cells were compared. The parasized HFF cells were cultured for 24 h, and the number of parasites in the vacuoles was determined by IFA. ($n = 3$ independent experiments, means ± SEM; $^{****}p \le 0.0001$, two-way ANOVA). **d** WT mice (ICR) or immune-deficient mice (BLAB/c nude) were infected with *DiCre* and *Δsdha* mutants (10^4 tachyzoites/mouse and 5 mice/strain). Parasite loads in peritoneal fluid were calculated by qPCR after 5 days of infection. The results are mean ± SEM. $^{****}p \le 0.0001$, Student's *t* test. **e** Virulence test of ICR mice infected with *DiCre* or *Δsdha* parasites (100 tachyzoites/mouse and 10 mice/strain). **f** Virulence test of ICR mice infected with a dose of 10^3 parasites of the specified strains (8 mice). The *Δsdha* mutant was also inoculated at higher doses (10^4, 10^5, 10^6 parasites/mouse; 5 mice/group). **g** Naive or *Δsdha*-immunized mice were infected with 10^4 RH-*Luc* tachyzoites (3 mice in each group). The parasite load of mice was analyzed by the IVIS Spectrum imaging system 5 days after RH-*Luc* infection. **h** The bioluminescence signal intensity of mice from (**g**) was calculated and plotted (means ± SEM; $^{****}p \le 0.0001$, Student's *t* test). **i** The survival of naive or *Δsdha* immunized mice infected with RH-*Luc*. **j** The survival of naive or *Δsdha*-immunized mice infected with ME49 tachyzoites (10^4).

the deletion of MDH. The plaque (Fig. 5b, c), replication (Fig. 5d) and virulence (Fig. 5e) assays displayed that loss of MDH had no discernible effect on the parasite. We were, therefore, promoted to consider alternative pathways that could supply malate to the cytoplasm. Tachyzoites encode a 2-oxoglutarate/malate translocase (OMT, TGGT1_274060), which may transport malate from the mitochondrion to the cytoplasm. Indeed, the HA-tagged OMT was expressed in the mitochondrion. Subsequently, the *Δomt* mutant was isolated by CRISPR/Cas9, pyrimethamine selection, screening PCR and immunostaining (Supplementary Fig. 5a, b). Deleting the *OMT* gene only slightly affected the tachyzoite growth, as evaluated by plaque, replication, virulence and parasite load assays (Supplementary Fig. 5c–f). The data imply a functional redundancy between OMT and MDH for supplying malate to the parasite cytosol.

Toxoplasma encodes a functional MDH-FAD located in mitochondria

Our data above describing cytoplasmic expression and the nonessential nature of MDH indicated the presence of an isoform for malate oxidation in the parasite mitochondrion. The database search identified a FAD-dependent malate-dehydrogenase (MDH-FAD). 10×HA fusion of the native MDH-FAD by 3′-genomic tagging disclosed a mitochondrial expression, co-localizing with HSP60 (Fig. 6a). *Tg*MDH-FAD was further

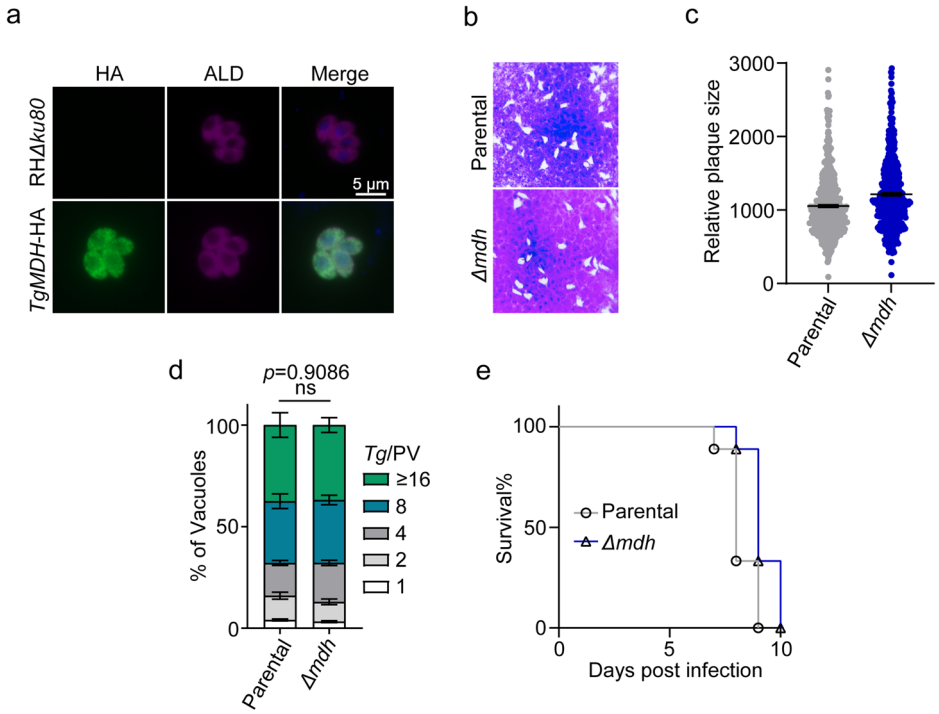

Fig. 5 | MDH is not required for the lytic cycle. **a** Construction of the MDH-HA localization strain from RHΔ*ku80*. MDH was found in the cytoplasm of *T. gondii*, co-localized with the characteristic cytoplasmic protein ALD. **b** The plaque size between parental and *Δmdh* was compared (7 d, 100 tachyzoites were used in each well, and 3 wells for each strain). **c** The relative size of the plaques from (**b**) (means ± SEM; Student's *t* test). **d** The replication assays of parental and *Δmdh* strains in HFF cells were compared. The strains infected with HFF cells were cultured for 24 h, and the number of parasites in the vacuoles was determined by IFA. **e** ICR mice were injected intraperitoneally with wild-type and *Δmdh* tachyzoites (100 parasites/mouse and 10 mice/strain).

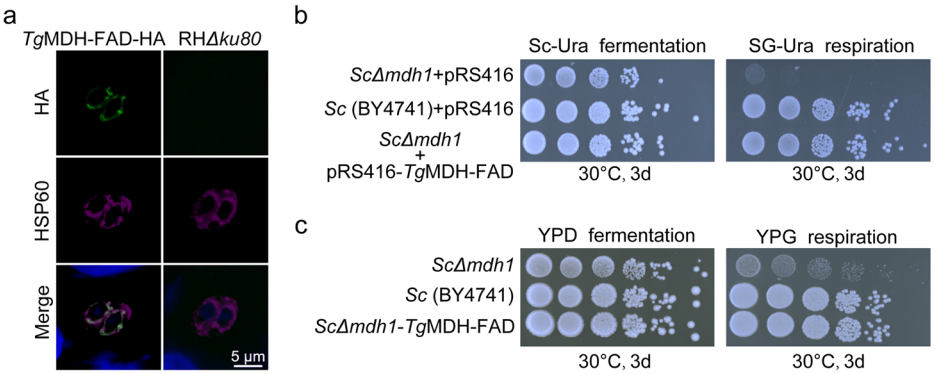

Fig. 6 | *Toxoplasma* expresses MDH-FAD in the mitochondrion. **a** Immunofluorescence assays were performed on the 10×HA-tagged strain to determine the localization of MDH-FAD. HSP60 was used as a marker specific to the mitochondrion for colocalization. **b** *Toxoplasma* MDH-FAD cDNA was amplified and cloned into the *pRS416*. The parental (BY4741) and *ScΔmdh1* strains transformed with the empty plasmid (*pRS416*) or construct (*pRS416*-MDH-FAD) were characterized on medium with glucose or glycerin as a sole carbon source by serial dilution assay. The plates were grown at 30 °C for 3 days. **c** The *Tg*MDH-FAD expressing mini gene was reintroduced into the chromosome of the *ScΔmdh1*. Growth of parental (BY4741), *ScΔmdh1* and *ScΔmdh1-Tg*MDH-FAD strains was tested either on glucose (YPD, fermentable carbon source) or on glycerol (YPG, non-fermentable carbon source) for 3 days at 30 °C.

examined by functional complementation of a *Saccharomyces cerevisiae* mutant (*ScΔmdh1*), which cannot grow on a non-fermentable carbon source[20]. As shown (Fig. 6b), the parental (BY4741) and *ScΔmdh1* strains transformed with the empty plasmid (*pRS416*) or construct (*pRS416*-MDH-FAD) were all able to grow on the fermentable carbon source. As expected, the mutant growth was restored by expressing *Tg*MDH-FAD, and *pRS416* failed to rescue its growth on glycerol (YPG, non-fermentable carbon source) (Fig. 6c). We constructed an *ScΔmdh-Tg*MDH-FAD strain expressing the parasite enzyme from chromosome XI to validate our results. Consistently, *Tg*MDH-FAD rescued the *ScΔmdh1* mutant on YPG plates (Fig. 6c), showing its functionality in yeast.

The MDH-FAD is required for the asexual reproduction of tachyzoites

In the next step, we investigated the metabolic relevance of MDH-FAD in tachyzoites. A pool of transgenic parasites expressing rapamycin-inducible dimerizable Cre (*DiCre*) and harboring loxP-flanked MDH-FAD (*Tg*MDH-FAD-cKD) was generated. Subsequently, a *Δmdh-fad* strain was produced by treating the *Tg*MDH-FAD-cKD strain with rapamycin (Supplementary Fig. 3c). The mutant was validated by PCR (Supplementary Fig. 3d), genome sequencing (Supplementary Fig. 4c) and immunofluorescence (Supplementary Fig. 3e) assay. Although the *Δmdh-fad* strain formed notably smaller plaques (Fig. 7a, b) and exhibited much smaller parasitophorous vacuoles (Fig. 7c), the *Δmdh-fad* mutant could be maintained in routine culture for a long time. In extended work, we infected mice with the *Δmdh-fad* strain and quantified the parasite load in the peritoneal fluid (Fig. 7d). Indeed, the deletion of MDH-FAD significantly reduced the parasite proliferation. Besides, mice parasitized by the *Δmdh-fad* mutant survived longer than those infected with the parental strain (Fig. 7e), indicating a reduced virulence upon deletion of *MDH-FAD*. These results emphasize the crucial function of MDH-FAD in promoting tachyzoite development in vitro and in vivo.

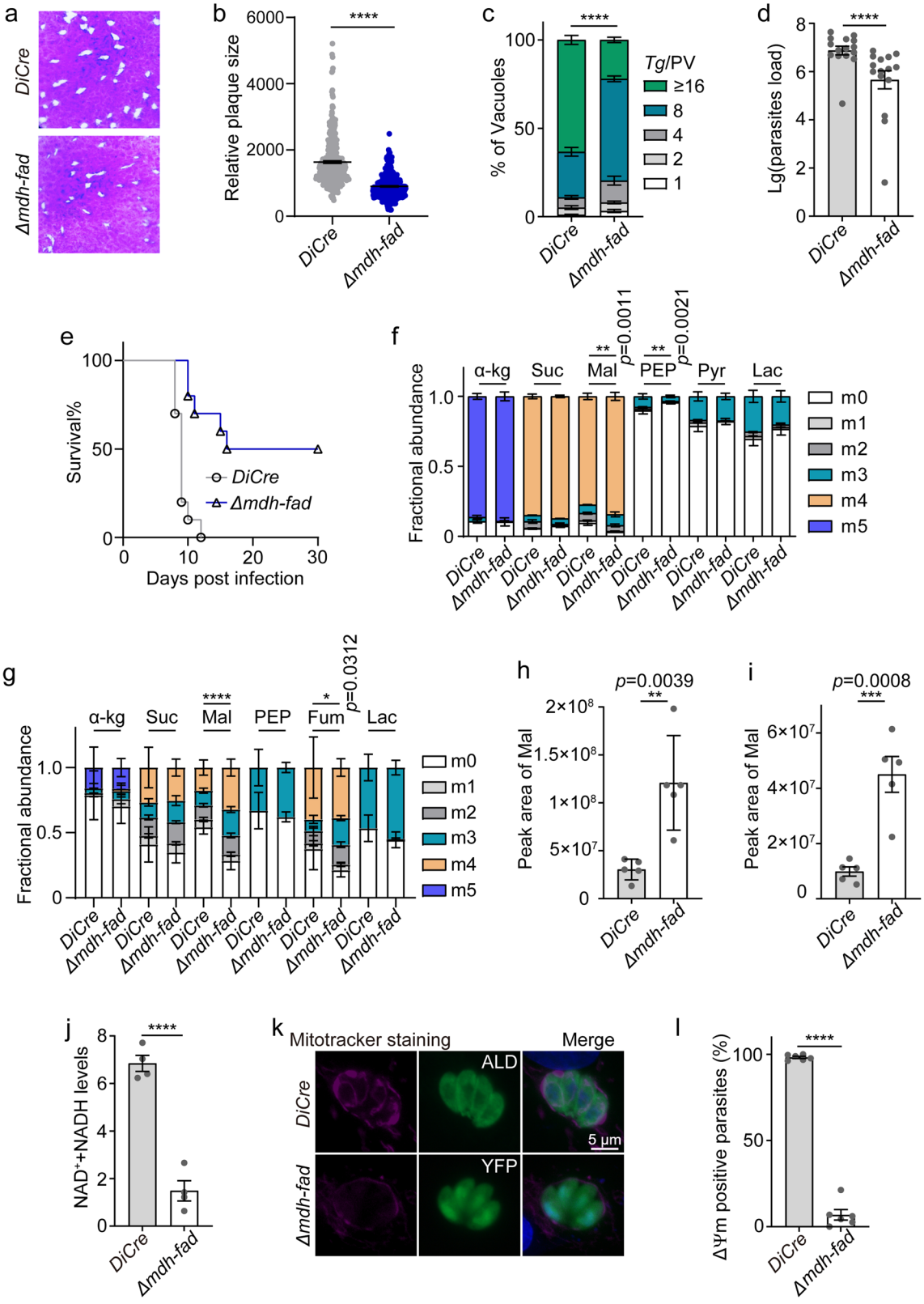

The *Δmdh-fad* strain displays impaired metabolism and membrane potential

To investigate whether deletion of *MDH-FAD* impacted the intermediates of the central carbon metabolism, we labeled extracellular tachyzoites of the *Δmdh-fad* and parental strains with [^{13}C]-glutamine for 4 h. We determined the inclusion of glutamine-derived carbon (^{13}C) into glycolytic and TCA metabolites using LC-MS. A change in ^{13}C labeling of α-ketoglutarate and succinate was not apparent (Fig. 7f). However, the tracer incorporation into malate was significantly increased (Fig. 7f). We also noted that the inclusion of glucose-derived ^{13}C into fumarate and malate was increased upon deleting *MDH-FAD* (Fig. 7g). As expected, the abundance of malate was considerably increased in the mutant (Fig. 7h). We observed a difference in

Fig. 7 | MDH-FAD is required for *T. gondii* growth. a The growth of *Δmdh-fad* and *DiCre* tachyzoites in vitro was compared by plaque assay (7 d, 100 tachyzoites/well and 3 wells for each strain). **b** The relative size of plaques from (**a**) (means ± SEM; ****$p \le 0.0001$, Student's *t* test). **c** The replication assays of *DiCre* and *Δmdh-fad* in vitro. After 24 h of infection with HFF cells, the number of parasites in vacuoles was determined by IFA. **d** Measurement of parasite burden in ICR mice. ICR mice were infected by intraperitoneal injection of *DiCre* and *Δmdh-fad* tachyzoites (10^4 tachyzoites/mouse and 5 mice/strain). Parasite loads in peritoneal fluid were calculated by qPCR after 5 days of infection. **e** ICR mice were injected intraperitoneally with wild-type and *Δmdh-fad* tachyzoites (100 parasites/mouse and 10 mice/strain). **f** *DiCre* and *Δmdh-fad* tachyzoites (5×10^7) were harvested and cultured for 4 h in a glucose-free medium supplemented with 8 mM $^{13}C_5$-glutamine. The levels of ^{13}C incorporation in glycolysis and TCA cycle metabolites were determined by the LC-MS. M0-M5 represents the number of carbons in the ^{13}C-labeled metabolites. Values are mean ± SEM of five independent experiments ($n = 5$, two-way ANOVA). **g** Incorporation of ^{13}C into glycolysis and TCA cycle metabolites, as determined by UHPLC-HRMS. The extracellular tachyzoites of the *DiCre* and *Δmdh-fad* strains were incubated with 8 mM $^{13}C_6$-glucose for 4 h ($n = 5$ biologically independent samples, means ± SEM; Student's *t* test). **h** Effect of *MDH-FAD* deletion on malate formation (data from panel (**f**)). The peak area represents the sum of M0-M4 peak areas (Student's *t* test). **i** Effect of *MDH-FAD* deletion on malate formation (data from panel (**g**)). The peak area represents the sum of M0-M4 peak areas (Student's *t* test). **j** The total of NAD^+ and NADH in *DiCre* and *Δmdh-fad* parasites was measured using a NAD^+/NADH assay kit. Means ± SEM from two independent experiments ($n = 2$), each with two replicates (****$p \le 0.0001$, Student's *t* test). **k** Mitotracker staining was used to examine the effect of *MDH-FAD* depletion on the membrane potential ($\Delta\psi m$). **l** The number of $\Delta\psi m$ positive tachyzoites in *DiCre* and *Δmdh-fad* strains was counted (****$p \le 0.0001$, Student's *t* test). The parental tachyzoites showed the typical intense staining of the mitochondrion and were classified as $\Delta\psi m$-positive.

malate labeling of the *Δmdh-fad* strain fed with [^{13}C]-glutamine and [^{13}C]-glucose (Fig. 7h, i). The glucose-derived ^{13}C into the TCA cycle requires oxaloacetate, whereas the influx of [^{13}C]-glutamine-derived carbon into malate is not dependent on oxaloacetate. A deletion of *MDH-FAD* may reduce the availability of oxaloacetate in the mitochondrion, resulting in a lower glucose-derived ^{13}C inclusion into malate. Our attempts to detect oxaloacetate in the parasites were unsuccessful, likely due to its rapid conversion to aspartate by aspartate aminotransferase (AST). We identified a mitochondrion-localized AST in *T. gondii*, as shown by the 10×HA gene fusion of the native AST (Supplementary Fig. 6a). The deletion of *AST* in the *DiCre* strain resulted in a notable reduction in plaque formation, replication, virulence, and parasite load (Supplementary Fig. 6b–g).

Interconversion of malate and oxaloacetate by MDH-FAD depends on NAD^+/NADH. We, therefore, measured the total NAD^+ and NADH levels in the mutant (Fig. 7j), which declined by about 80% upon loss of MDH-FAD expression. Because NADH is an electron donor in the inner mitochondrial membrane, we examined the membrane potential ($\Delta\psi m$) using mitotracker staining (Fig. 7k). Intracellular tachyzoites of the parental strain had well-stained mitochondrion, classified as $\Delta\psi m^+$(Fig. 7l). In contrast, mitochondrial staining was not detectable in over 80% of the *Δmdh-fad* parasites (Fig. 7l), signifying a collapse of $\Delta\psi m$ in the organelle upon deletion of *MDH-FAD*.

The ME, localized in the nucleus, is essential for parasite development

Our follow-up work focused on ME, which catalyzes malate to pyruvate while producing NADPH. We first determined its subcellular localization using antisera and by ectopic expression of epitope-tagged ME (Fig. 8a, b). Immunofluorescent staining showed that ME co-localized with Hoechst (DNA dye, Fig. 8a, b). In the next step, we made a conditional mutant of ME using the auxin-inducible degron (AID) system (Supplementary Fig. 3f) because its knockout *via* CRISPR/Cas9-mediated homologous replacement was not feasible. PCR screening of the drug-resistant parasite clones identified a miniAID-ME mutant (Supplementary Fig. 3g), in which the protein could be rapidly degraded by indole-3-acetic acid (IAA, Fig. 8c). A knockdown of ME resulted in reduced plaque size (Fig. 8d) and smaller vacuole size distribution (Fig. 8e). Besides, the ICR mice infected by the miniAID-ME tachyzoites (10^4, i.p.), followed by treatment with IAA in drinking water, demonstrated a highly-reduced parasite load compared to the untreated control (-IAA) and the parental strain (Fig. 8f). These results underline the critical role of ME in tachyzoite propagation.

The ME-depleted strain exhibits a selective perturbation of transcriptome

ME produces pyruvate from malate, a crucial precursor for several metabolic pathways in the cytoplasm, apicoplast, and mitochondrion[12]. While not known in *T. gondii*, pyruvate metabolism in the nucleus is critical for histone acetylation and chromatin remodeling in mammalian cells[21,22]. To determine whether the ME depletion impacts histone acetylation in tachyzoites, we conducted an immunofluorescence analysis using the specificity of the H3K9ac-directed antibodies (Fig. 8g). Our findings revealed that ME depletion markedly decreased the H3K9ac signal intensity in the parasite nucleus (Fig. 8h), indicating that ME-derived pyruvate plays a pivotal role in acetyl-CoA synthesis for epigenetic regulation in tachyzoites.

The miniAID-ME strain was grown with or without IAA for 12 h, and then samples were collected for RNA sequencing to assess the global consequences of ME knockdown. The ME-depleted strain exhibited a lower expression of 2342 transcripts, while 1731 were more abundant (Supplementary Fig. 7a). Several histone deacetylases and histone acetyltransferases, including HDAC1, HDAC2, HDAC5, SiR2, MYST, GCN5, and GNAT family protein, displayed dysregulated expression (Supplementary Fig. 7b). The qPCR verified the lower expression of SIR2 and more abundance of GCN5-B, HDAC5 and MYST-B transcripts in the ME-depleted mutants (Supplementary Fig. 7c). Furthermore, KEGG enrichment analysis revealed that DNA replication, mismatch repair and amino sugar and nucleotide sugar metabolism were the most significantly affected in instances where ME expression was lacking (Supplementary Fig. 7d).

Nuclear localization of ME is imperative for tachyzoite growth

ME comprises the N-terminal, Tudor, and C-terminal domains (Fig. 9a). Notably, the C-terminal contains two nuclear localization signals (Fig. 9a). To determine the functional relevance of these domains, we complemented the miniAID-ME strain by the N-terminal domain, both the N- and C-terminal domains, or the complete open reading frame of ME at the *UPRT* locus (Fig. 9b). A diagnostic PCR of each strain confirmed the integration of the respective insert (Supplementary Fig. 8a–c, comp-ME, comp-ME-N/C, comp-ME-N). Immunostaining revealed a nuclear localization in the comp-ME and comp-ME-N/C strains (Fig. 9c). In contrast, the comp-ME-N strain showed a cytosolic expression (Fig. 9c), indicating a role of the C-terminal in the nuclear transport of ME. As anticipated, the comp-ME strain displayed a fully restored lytic cycle (plaque formation, Fig. 9d) and replication (Fig. 9e) in the IAA-treated/ME-depleted mutant. A recovered phenotype of the comp-ME-N/C strain (+IAA) suggested a nonessential nature of the Tudor domain. Unlike the nuclear-localized constructs, the IAA-exposed comp-ME-N strain could not grow (Fig. 9d, e), highlighting the importance of ME expression in the parasite nucleus.

Discussion

Herein, we demonstrate the network design of carbon metabolism in the mitochondrion and nucleus of a globally prevalent and clinically relevant human and animal pathogen, *Toxoplasma gondii*. Our integrative approach discloses previously unknown plasticity, inter-organelle cooperativity, vulnerability and therapeutic potential of major metabolic enzymes in the parasite mitochondrion, cytosol and nucleus (Fig. 10).

We show a significant role of the mitochondrial isoform of citrate synthase (CS1) for in vitro growth of tachyzoites and in vivo virulence. A

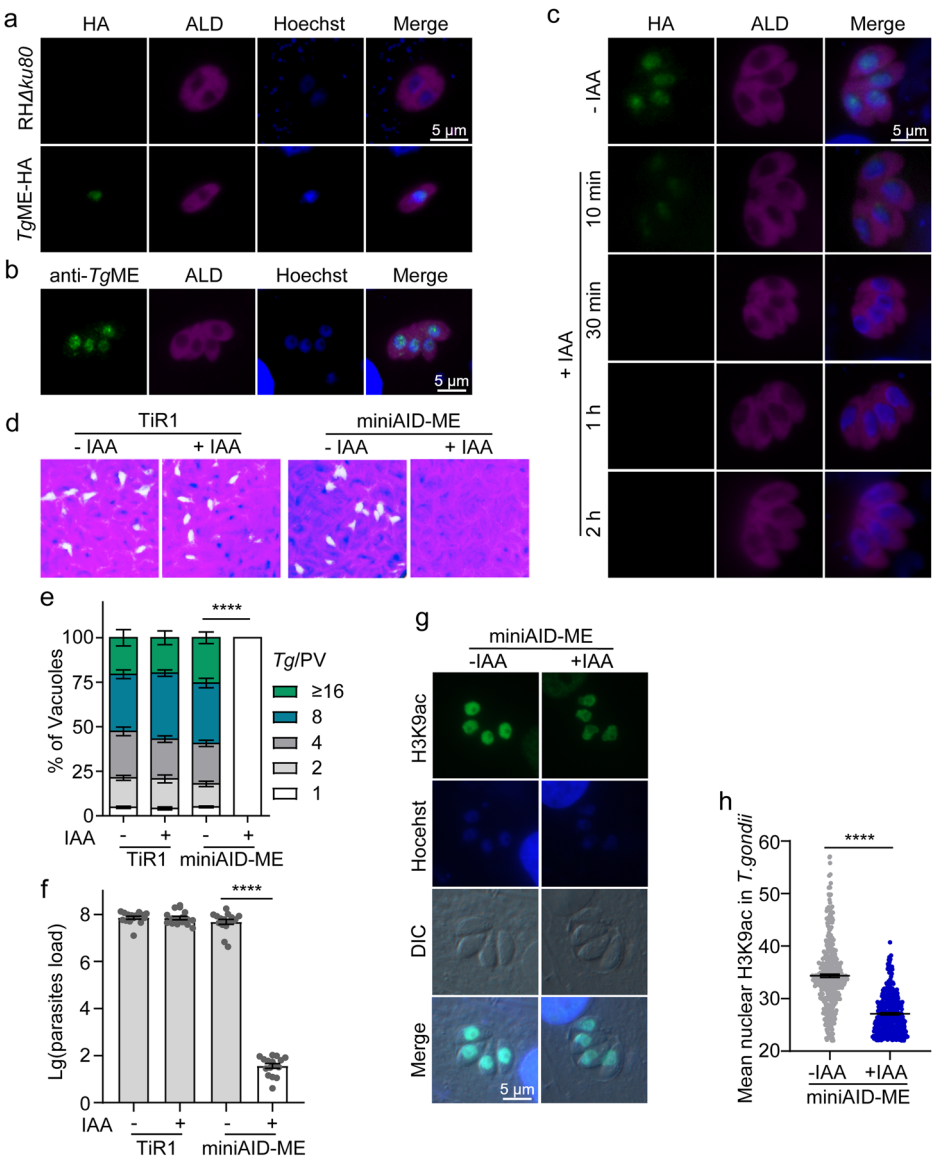

Fig. 8 | ME is critical for the lytic cycle of tachyzoites. a Immunofluorescent microscopic analysis of ME. Hoechst is a cell nucleus marker. **b** Immunofluorescence detection of co-localization of native ME with the nucleus marker, Hoechst. **c** Immunofluorescent localization and regulation of ME by indole-3-acetic acid (IAA). Intracellular miniAID-ME tachyzoites cultured in the absence or presence of 500 μM IAA were stained by α-HA and α-ALD antibodies. **d** The growth of TiR1 (RHΔ*ku80*-TiR1) and miniAID-ME tachyzoites was compared by plaque assay (−/+500 μM IAA, 7d, 100 tachyzoites/well and 3 wells for each strain). **e** Intracellular growth of TiR1 and miniAID-ME strains (−/+500 μM IAA, 24 h, means ± SEM, $n = 3$ independent experiments. $^{****}p \le 0.0001$, two-way ANOVA). **f** ICR mice were infected with TiR1 and miniAID-ME tachyzoites by intraperitoneal injection (10^4 tachyzoites/mouse and 5 mice/strain). IAA was added to the drinking water or not. After 5 days of infection, parasite loads in peritoneal fluids were calculated by qPCR based on the 529 gene, $^{****}p \le 0.0001$, Student's *t* test. **g**, **h** Immunostaining and quantification of histone acetylation in the parasite nucleus. Analyses were performed using rabbit anti-H3K9ac antibody, and the fluorescence intensity was quantified. Each symbol in panel (**h**) marks the pixel density of a parasite nucleus (means ± SEM, $n = 3$ assays. $^{****}p \le 0.0001$, Student's *t* test).

similar outcome was reported recently[23]. Our study revealed a more pronounced reduction in virulence of the *Δcs1* mutants, which may be attributed to the disparate genetic backgrounds of the parental strains. The depletion of *CS1* partly phenocopies the mutants of MPC1 and MPC2 transporting glycolysis-derived pyruvate into the mitochondrion and BCKDH-E1α subunit facilitating acetyl-CoA synthesis from MPC-imported pyruvate. These knockout strains are not lethal to the parasite survival in vitro, but exhibit varying degrees of attenuation in their virulence in mice[8,14]. It has been reported that the mitochondria-localized 2-methylcitrate synthase (PrpC) has citrate synthase activity, although the catalytic efficiency of CS1 is notably higher than that of PrpC[23]. Consequently, when *CS1* is knocked out, PrpC may facilitate citrate formation from acetyl-CoA, thereby maintaining the functionality of the TCA cycle (Fig. 10). *T. gondii* also expresses a CS2 in the cytoplasm, producing citrate[23], which is hypothesized to be transported into the apicoplast and subsequently serve as a substrate for ACO to generate isocitric acid. The latter is metabolized by IDH2 to produce α-ketoglutarate and NADPH, contributing to FASII pathways in the organelle (Fig. 10). This premise is supported by the evidence that the parasite encodes an aconitase (ACO) and two isocitrate dehydrogenases (IDH1 and IDH2). The ACO is dual-localized in the mitochondrion and the apicoplast[24], whereas The IDH1 and IDH2 are present in the mitochondrion and apicoplast, respectively[15]. Whether CS2-derived citrate can traffic to the apicoplast and mitochondrion to support biosynthetic pathways in both organelles requires additional research.

SCSα and SSADH may synergize to supply succinate to the cycle (Fig. 10). A notably mild phenotype of the *Δssadh* mutant suggests that the GABA-derived succinic semialdehyde is not a significant contributor of succinate. Similarly, loss of GABA-AT, which converts GABA to succinic semialdehyde, does not affect parasite growth[16]. By contrast, the *Δscsα* strain exhibited a more severe phenotype which indicates its primary function in supplying succinate. However, the *Δscsα* mutant could be maintained in culture, suggesting that SSADH may compensate for succinate, albeit not sufficiently to ensure normal growth without *SCSα*. A double deletion of *SSADH and SCSα* further detrimented parasite growth but the mutant was viable in culture. We postulate that propionate-derived succinate *via* the 2-methylcitrate cycle[25] may partly fuel the TCA cycle in tachyzoites (Fig. 10).

We also found that *SDHA* is vital for parasite growth, and the *Δsdha* mutant is avirulent in mice. Our attempts to delete the FH protein, converting SDHA-derived fumarate to malate, were unsuccessful, indicating its crucial role for the growth of *T. gondii*. Interestingly, FH-deficient *Plasmodium berghei* is viable[26]. A conditional mutant of FH in tachyzoites of *T. gondii* is required to define its role better. Besides $PEPCK_{mt}$[11], MDH-FAD likely enables the parasite to reprogram its oxaloacetate supply in varying milieus (Fig. 10). It can complement a *Δmdh1* yeast mutant impaired in

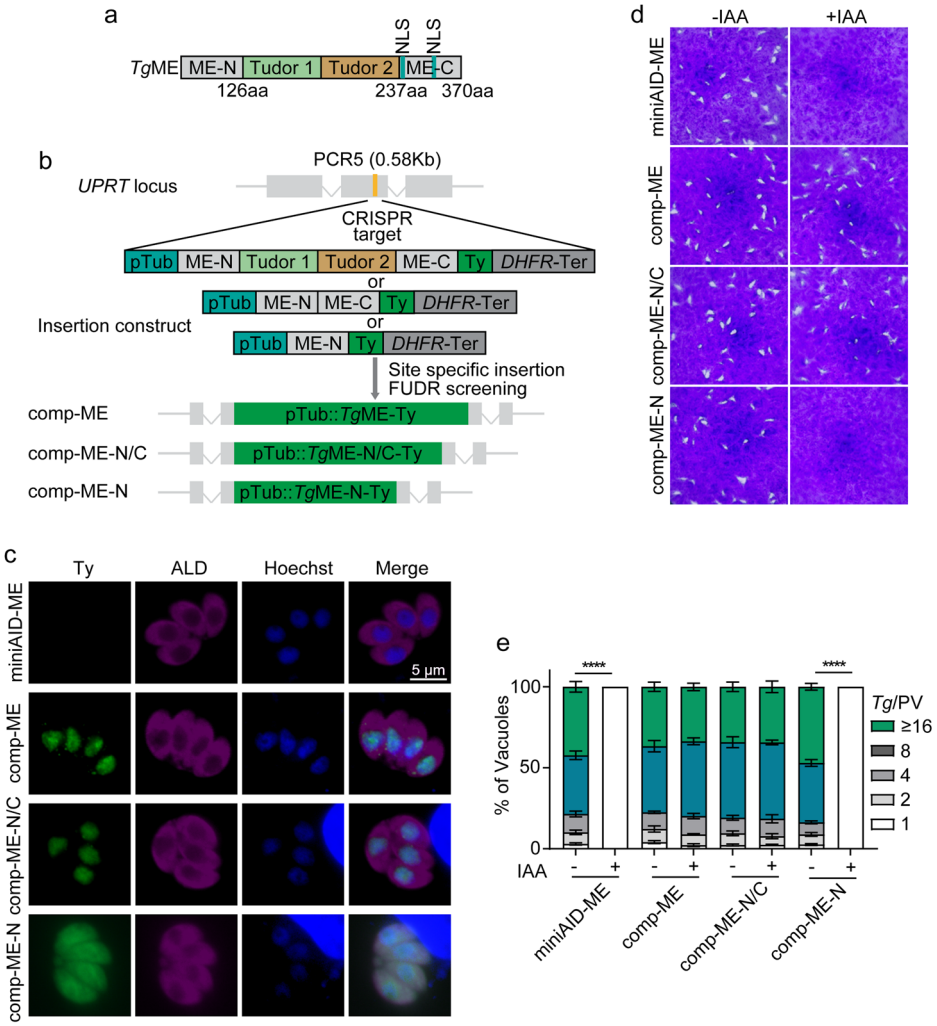

Fig. 9 | Functional analysis of the ME domain. **a** The ME comprises the N-terminal, Tudor1, Tudor2, and C-terminal domains. The nuclear localization signal (NLS) of ME was analyzed using https://www.novoprolabs.com/tools/nls-signal-prediction. **b** The domains were expressed in the *UPRT* locus of miniAID-ME to create the comp-ME, comp-ME-N/C, and comp-ME-N mutants. **c** The expression of ME-Ty, ME-N/C-Ty and ME-N-Ty were confirmed by IFA using an anti-Ty antibody. **d** Plaque assays were carried out under −/+500 µM IAA for 7 days. **e** The parasites were subjected to intracellular replication assays under specified conditions. ($n = 3$ independent assays, means ± SEM; $^{****}p \leq 0.0001$, two-way ANOVA).

growth on glycerol (non-fermentable carbon source), and the *Δmdh-fad* tachyzoite shows a mild phenotype. The mutant accumulates malate, its NADH pool is severely compromised and the mitochondrial membrane potential collapses. Despite such metabolic anomalies, the mere survival and virulence of the *Δmdh-fad* mutant is unprecedented. We believe $PEPCK_{mt}$ may offset the deficiency of oxaloacetate[11], and ATP can be supplied through glycolysis and salvage pathways. Indeed, tachyzoites express an ATP carrier (AAC1) in the mitochondrion[27,28] and can acquire host-derived ATP[29]. However, there appears to be no substitute mechanism for maintaining the NADH and membrane potential in the *Δmdh-fad* mutant. The adaptive reprogramming in the *Δmdh-fad* strain warrants further investigation.

A second isoform of MDH is expressed in parasite cytosol, indicating the presence of a malate-aspartate shuttle for the transfer of $NADH/NAD^+$ to the mitochondrion (Fig. 10). Previous work showed the myc-tagged MDH localizing to the mitochondrion of *T. gondii*[15]. However, our findings indicate that MDH-HA co-localizes with the cytoplasmic protein ALD. Consistent with our finding, the location of MDH was predicted to be in the cytoplasm by HyperLOPIT[30]. This discrepancy in the localization of MDH can be attributed to the use of different transgenic approaches. The *Δmdh* mutant shows no growth phenotype, and therefore seems dispensable for malate synthesis. Tachyzoites encode a 2-oxoglutarate/malate translocase (OMT, TGGT1_274060) located in the mitochondrion-membranes[30], which could potentially compensate for the loss of cytosolic MDH. On the other hand, the malic enzyme, producing NADPH and pyruvate in the nucleus, is essential. NADPH is required for cellular processes, including nucleotide biosynthesis and redox balance. Likewise, acetyl-CoA synthesis from pyruvate in the nucleus is vital for histone acetylation and chromatin remodeling[21,22]. Our transcriptomics data displayed that conditional knockdown of ME is associated with the modulation of replication, mismatch repair, amino sugar and nucleotide sugar metabolism. Loss of ME did not impact the total NADPH, likely due to other NADPH-generating pathways, including oxidative pentose phosphate pathway (oxPPP) and folate metabolism[31,32].

Previous research indicated that Tudor domain proteins are molecular adaptors involved in RNA metabolism, DNA damage response, and chromatin modification[33–35]. However, it is noteworthy that we could rescue the ME-depleted strain by complementing the C-terminus and N-terminus, excluding the Tudor domain. Our data also show that the ME expression in the nucleus is regulated *via* the C-terminal, and its nuclear expression is essential for the lytic cycle. In mammalian cells, increasing evidence shows nuclear-mitochondrial crosstalk involving the translocation of metabolic enzymes[36]. There is even relocation of pyruvate dehydrogenase complex to the nucleus and the occurrence of a nuclear TCA cycle regulating the metabolic-epigenetic circuitry[21,22,37]. It is, therefore, tempting to surmise a role of ME-derived pyruvate in acetyl-CoA synthesis for epigenetic regulation in tachyzoites – a premise supported by our initial studies of histone acetylation. Future work shall focus on yet-uncharacterized isoforms of metabolic enzymes to study the nuclear metabolism and mito-nuclear crosstalk in *T. gondii*. Lastly, ME, SCSα and SDHA emerge as potential therapeutic targets against acute toxoplasmosis.

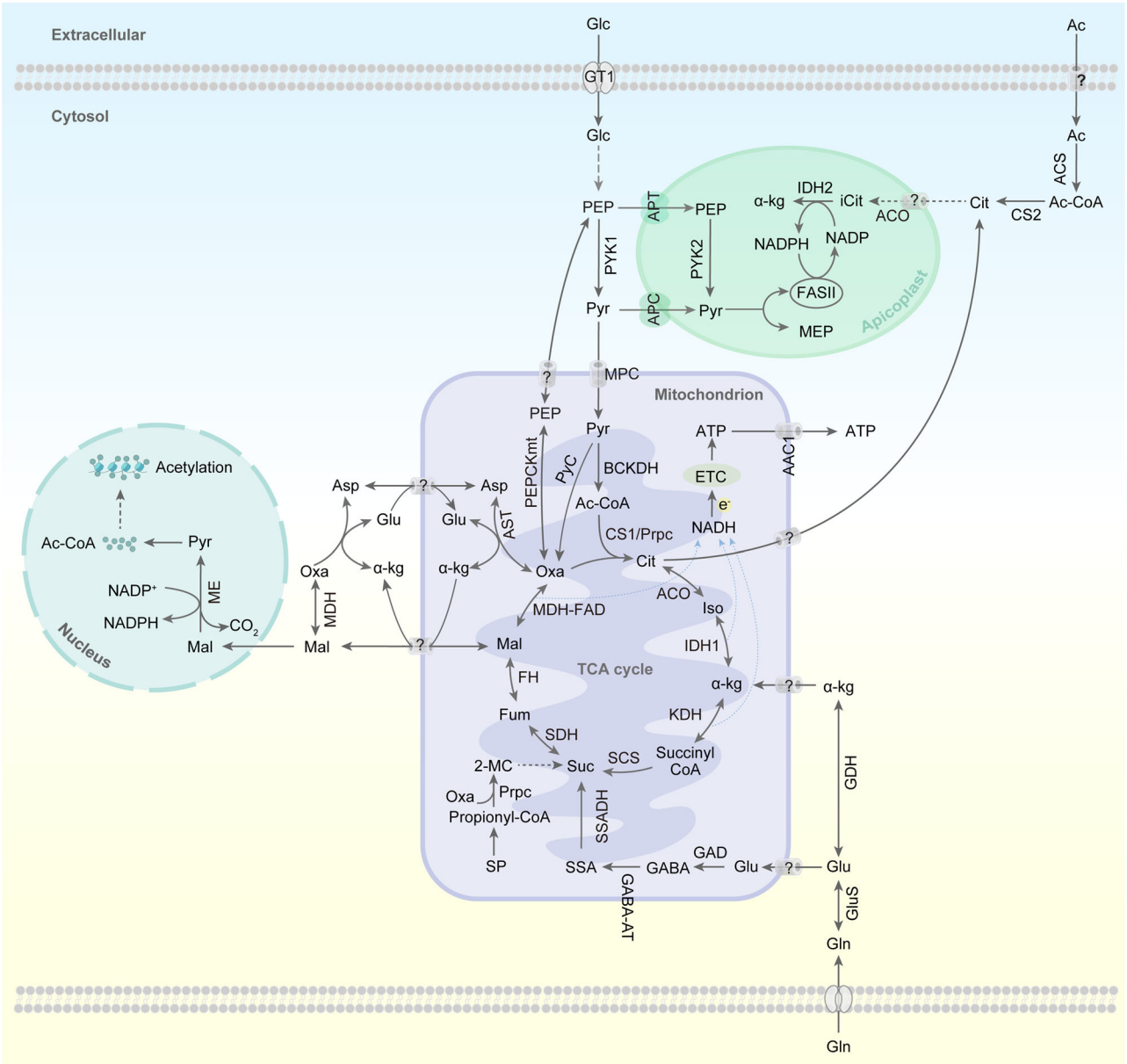

Fig. 10 | Mito-nuclear carbon metabolism in *Toxoplasma*. *Toxoplasma* actively catabolizes host glucose *via* a canonical TCA cycle and also catabolizes glutamine *via* the GABA shunt and TCA cycle. Mitochondrial-localized MDH-FAD may participate in the TCA cycle, whereas cytoplasmic-localized MDH mediates the interconversion of oxaloacetate and malate. Malate is utilized by ME in the nucleus to produce pyruvate, a step that is essential for the growth and survival of *Toxoplasma*. The question mark denotes the to-be-identified transporters in the mitochondrion, apicoplast or plasma membranes. Glc glucose, GT1 glucose transporter, PEP phosphoenolpyruvate, Pyr pyruvate, PYK1 pyruvate kinase 1, PYK2 pyruvate kinase 2, APT apicoplast phosphate translocator, APC apicoplast pyruvate carrier, MEP methylerythritol 4-phosphate pathway, FAS II type II fatty acid synthesis pathway, MPC mitochondrial pyruvate carrier, BCKDH branched-chain α-ketoacid dehydrogenase, PyC pyruvate carboxylase, Ac-CoA acetyl-CoA, Cit citrate, iCit isocitrate, α-KG α-ketoglutarate, CS1 citrate synthase 1, CS2 citrate synthase 2, PrpC 2-methylcitrate synthase, ACO aconitase, Iso isocitric acid, IDH1 isocitrate dehydrogenase 1, IDH2 isocitrate dehydrogenase 2, KDH α-ketoglutarate dehydrogenase, SCS succinyl-CoA synthetase, SSADH succinic semialdehyde dehydrogenase, Suc succinate, Fum fumarate, SDH succinate dehydrogenase, FH fumarase, Mal malate, MDH-FAD FAD malate-dehydrogenase, MDH malate dehydrogenase, Oxa oxaloacetate, ME malic enzyme, PEPCK phosphoenolpyruvate carboxykinase, AST aspartate aminotransferase, Asp aspartate, Gln glutamine, Glu glutamate, GluS glutaminase, GDH glutamate dehydrogenase, GAD glutamate decarboxylase, GABA γ-aminobutyric acid, GABA-AT gamma-aminobutyric acid-aminotransferase, SSA succinic semialdehyde, SP sodium propionate, Ac acetate, ACS Acetyl-CoA synthetase, NADH nicotinamide adenine dinucleotide, NADPH nicotinamide adenine dinucleotide phosphate, ETC electron transport chain, ATP adenosine triphosphate, AAC1 mitochondrial ADP/ATP Carrier 1, TCA cycle tricarboxylic acid cycle.

Materials and methods

Biological resources and ethics statement

The RH*Δku80*[38], RH*Δku80*-TiR1, RH DiCre_T2A *Δku80Δhxgprt* (*DiCre*)[39–41], RH_*Luc* and ME49 strains were provided by Bang Shen (Huazhong Agricultural University, Wuhan), respectively. Indole-3-acetic acid (IAA) was purchased from Sigma-Aldrich. Anti-Ty (mouse), anti-HSP60 (mouse), and anti-ALD (rabbit) antibodies were provided by Bang Shen (Huazhong Agricultural University, Wuhan). Anti-HA (mouse, Cat#M180-3) was purchased from MBL (Medical & Biological Laboratories Co., Japan). Rabbit anti-H3K9ac antibodies (Cat#9649) were purchased from CST (Cell Signaling Technology, USA). Alexa Fluor 488 (Cat#4408) and Alexa Fluor 594 (Cat#8889) antibodies were purchased from CST (Cell

Signaling Technology, USA). Hoechst dye (Cat#94403) were purchased from Sigma-Aldrich. The female ICR mice (six-week-old) were obtained from the Guangdong Medical Experimental Animal Center (Guangdong, China). The Balb/c-nu mice were acquired from Guangzhou Ruige Biotechnology Co., LTD. We have complied with all relevant ethical regulations for animal use. Animals were raised under standard conditions approved by the Ethics Committee of South China Agricultural University (Permit 2023f266).

Cell culture

Genetically modified strains were generated using the RH*Δku80*[38], RH*Δku80*-TiR1 and *DiCre* as the parental strains[39–41]. Parasites were propagated in human foreskin fibroblasts (HFF) (ATCC, USA) using Dulbecco's modified Eagle's medium (DMEM) supplemented with 2% fetal bovine serum, 4500 mg/L glucose, 2 mM glutamine, 10 U/mL penicillin and 100 μg/mL streptomycin.

Making of transgenic parasites

Supplementary Tables S1 (Supplementary Data 1) and S2 (Supplementary Data 2) describe primers and plasmids deployed in this study. The CRISPR/Cas9 plasmid was constructed using pEASY-Basic Seamless Cloning and Assembly Kit (TransGen Biotech, China). Other plasmids were constructed using the ClonExpress II one-step cloning kit (Vazyme Biotechnology, China). For 3'-genomic tagging, we amplified the 10×HA sequence flanked by homologous arms of the target gene and co-transfected it with the matching CRISPR/Cas9 constructs into the RH*Δku80* or *DiCre* strain. Transgenic strains were selected with 1 μM pyrimethamine (Sigma Aldrich, USA) and identified through diagnostic PCR and indirect immunofluorescence (IFA) assays. The *CS1* (TGGT1_268890), *SSADH* (TGGT1_257480), *SCSα* (TGGT1_290600), *SDHA* (TGGT1_215590), *MDH* (TGGT1_318430), *OMT* (TGGT1_274060), *AST* (TGGT1_248600) and *MDH-FAD* (TGGT1_288500) knockout strains (Supplementary Data 3) were generated by co-transfecting YFP-*DHFR** or *DHFR** cassettes flanked by homologous arms of the corresponding target genes and CRISPR/Cas9 constructs into the *DiCre* strain. The strains were selected with 1 μM pyrimethamine, cloned by limiting dilution and clonal strains were screened by diagnostic PCRs and the YFP^+ signal. The *ΔscsαΔssadh* strain was generated by replacing *SSADH* with Tub-CAT-mCherry *via* the CRISPR/Cas9 method and chloramphenicol selection (30 μM, Sigma-Aldrich, USA). The double mutant was isolated by diagnostic PCR screening and the $mCherry^+$ signal.

The conditional knockdown strain for ME (TGGT1_286440) was generated by co-transfecting the locus-specific CRISPR/Cas9 construct and homology donor template into the RH*Δku80*-TiR1 strain (refer Supplementary Data 2), followed by selection with 25 μg/mL mycophenolic acid and 50 μg/mL xanthine. Degradation of ME in the eventual mutant (miniAID-ME) was induced by 500 μM IAA. The miniAID-ME strain was used further to generate the comp-ME, comp-ME-N/C and comp-ME-N strains by inserting the specific expression cassette into the *UPRT* locus (selection with 10 μM 5-fluorodeoxyuracil). Clonal strains were identified by diagnostic PCRs and IFA.

TgMDH-FAD complementation in *S. cerevisiae*

The empty vector (*pRS416*) and the indicated *TgMDH-FAD* construct (*pRS416-MDH-FAD*) were transformed into the *ScΔmdh1* mutant. Briefly, the *ScΔmdh1* strain was grown in 2% yeast extract, 1% tryptone, and 2% glucose. Following transformation with the plasmids described above, all yeast strains were cultured in synthetic dropout (uracil-free) minimal medium (0.67% yeast nitrogen base) supplemented with appropriate amino acids and 2% glucose. The transfectants were cloned on selective plates and tested for growth complementation on a medium with glucose or glycerin as a sole carbon source by serial dilution assay (30 °C for 3 days). The *Tg*MDH-FAD expression cassette was introduced into chromosome XI of the *ScΔmdh1*. Clonal strains were selected on plates and tested for growth complementation on a medium with glucose or glycerin as a sole carbon source by serial dilution assay (30 °C for 3 days).

Production of polyclonal antibodies

The open reading frames of ME were amplified from the RH*Δku80* strain and cloned into the *pCold* vector containing a 6×His tag. The *pCold-ME* construct was transformed into the BL21(DE3) strain of *E. coli*, and protein expression was induced by IPTG. The recombinant proteins were purified *via* Ni-NTA affinity resin and used to immunize female mice (six-week-old). The purified protein preparation and positive sera were aliquoted and stored at −80 °C.

Immunofluorescence assays

Based on a protocol described previously[42], HFF cells were infected by the parental and transgenic strains and then fixed with 4% paraformaldehyde (15 min), permeabilized with 0.1% Triton X-100 (20 min) and blocked with 10% FBS (2 hours). Samples were treated with mouse anti-HA (1:1000), rabbit anti-ALD (1:1000) and rabbit anti-H3K9ac antibodies (30 min, 1:400) and stained with Alexa Fluor488 (goat anti-mouse, 1:1000), Alexa Fluor594 (goat anti-rabbit, 1:1000) IgG and Hoechst dye (30 min, 1:1000). Parasitized cells were imaged using a BX53 fluorescence microscope (Olympus, Japan) or ZEISS LSM 980 with Airyscan 2 (Carl Zeiss, Germany) and refined using ZEN software (Carl Zeiss, Germany). Image J software was used to process the fluorescent images.

Parasite phenotyping

Plaque assay were set up in 6-well plates seeded with HFF cells (100 tachyzoites/well, 3 wells per strain), essentially as reported earlier[43]. Cultures were incubated unperturbed at 37 °C and 5% CO_2 for 6–10 days. Samples were fixed with 4% paraformaldehyde (20 min), washed by PBS, stained with 0.1% crystal violet (20 min) and scanned (Microtek Scan Marker i600, Microtek, China) to analyze the plaque size. To assess the replication efficiency, HFFs were infected with parental (RH*Δku80*-TiR1) or miniAID-ME strains preincubated for 2 h with or without 500 μM IAA. Cells were fixed using 4% paraformaldehyde and then incubated with mouse anti-*Tg* IgG (30 min). Samples were permeabilized by 0.1% Triton X-100 (20 min) and blocked with 10% FBS (2 h). Subsequently, they were incubated with rabbit anti-ALD (30 min, 1:1000), followed by Alexa Fluor 488 (goat anti-mouse, 1:1000) and Alexa Fluor 594 (goat anti-rabbit, 1:1000), and Hoechst (1:1000) was used for 30 min. The *DiCre* and *Δmdh* parasites were immunostained by mouse anti-*Tg* IgG (before permeabilization, 1:1000) and rabbit anti-ALD (after permeabilization, 1:1000) to visualize non-invaded and total parasites, respectively. The *Δcs1*, *Δssadh*, *Δscsα*, *ΔscsαΔssadh*, *Δsdha* and *Δmdh-fad* parasites were visualized by YFP^+ signal and mouse anti-*Tg* IgG (1:1000), followed by Alexa Fluor 594 (goat anti-mouse, 1:1000). At least 100 vacuoles per sample were scored for the number of parasites developing within them.

NAD^+/NADH measurement

Freshly isolated tachyzoites of the *DiCre* and *Δmdh-fad* strains were lysed in 200 μL of NAD^+/NADH extraction buffer on ice (30 min) and centrifuged at 12,000 *g* (10 min). The total NAD^+ and NADH levels in the supernatant were detected using an NAD^+/NADH assay kit with WST-8 (Beyotime, Shanghai, China)[44]. Briefly, a 20 μL sample or NADH standards (0–20 μM) was added to a 96-well plate. Subsequently, 90 μL of alcohol dehydrogenase was added and incubated at 37 °C (10 min), followed by the addition of 10 μL chromogenic solution (37 °C, 45 min). The absorbance values were determined at 450 nm using a plate reader (Synergy, BioTek Instruments, USA).

Parasite virulence and burden

The female ICR mice were infected with extracellular parasites of the specified strains by intraperitoneal injection (100 tachyzoites/mouse, 10 mice/strain). Infection by the *Δscsα* mutant was performed at doses of 10^3, 10^4

parasites (8 mice/group) and 10^5, 10^6 parasites (5 mice/group). The clinical signs and survival were monitored daily, and blood samples were collected from the surviving mice. Seronegative animals were not included in the data analysis[45,46]. To determine the parasite proliferation, we infected female ICR or Balb/c-nu mice by intraperitoneal injection (10^4 parasites, 5–6 mice/strain). Animals infected with the *Δcs1*, *Δssadh*, *Δscsα*, *Δsdha*, *Δmdh-fad*, and *DiCre* strains were provided with normal purified water, while those harboring the RH*Δku80*-TiR1 and miniAID-ME strains were given water with or without 500 μM IAA. Peritoneal fluids were collected 5 days post-infection, and genomic DNA was extracted using the TIANamp Blood DNA Kit from Tiangen Biotechnology Co., Ltd. (China). Parasites in the peritoneal fluids were detected by amplifying the non-coding fragment (529 bp, primers in Supplementary Data 1) using Power SYBR Green PCR Master Mix from Toyobo Co., Ltd. (Japan)[45,46].

Bioluminescence imaging

ICR mice were immunized with the *Δscsα* or *Δsdha* mutant (10^2) *via* intraperitoneal injection. 34–39 days post-immunization, mice were infected with the luciferase-expressing RH-*Luc* strain (10^4 tachyzoites/animal, 3 or 4 mice/group, i.p.). Naïve mice were inoculated with the same dose of the indicated strains as control groups (3 or 4 mice/group, i.p.). Animals were anesthetized (1.25% tribromoethanol, MeilunBio Co., Ltd, China) five days after infection and 300 μL of 15 mg/mL D-luciferin was injected intraperitoneally (Yeasen Biotechnology Co., Ltd, Shanghai, China). The IVIS spectrum imaging (PerkinElmer, USA) was performed to detect the parasite load[47].

Genomics and transcriptomics

The *Δcs1*, *Δmdh* and *Δmdh-fad* tachyzoites were purified, and genomic DNA was extracted using the TIANamp Blood DNA Kit (Tiangen Biotechnology Co., Ltd., China). The genome was then sequenced as reported previously[48]. The curated datasets were compared to the reference genome of the GT1 strain (ToxoDB), and the results were visualized using the integrated genome viewer. For transcriptomics, the miniAID-ME strain was pre-treated with −/+500 μM IAA for 12 h, and parasites were purified. Total RNA was extracted using Transzol UP reagent (TransGen Biotech Co., Ltd., China). RNA sequencing was performed as described before[49]. The transcriptome datasets were analyzed using the Majorbio Cloud Platform (www.majorbio.com).

Metabolomics

Metabolic labeling of extracellular tachyzoites with stable isotopes of glucose or glutamine was carried out following a modified method described previously[10,11]. Tachyzoites (5×10^7) of the *DiCre* and *Δmdh-fad* strains were cultured for 4 hours in a glucose-free medium containing 8 mM $^{13}C_6$-glucose or $^{13}C_5$-glutamine. Subsequently, parasites were washed with PBS and treated with 1 mL of ice-cold methanol (80%)[50]. Samples were sonicated (5 cycles, 1 min each with intermittent ice cooling) and stored at −20 °C for 30 min.

Metabolites were extracted by sample centrifugation, and the supernatant was evaporated to dryness. The residue was reconstituted in 100 μL of water and then mixed with 50 μL of 175 mM 3-NPH (Sigma Aldrich, USA) in 75% methanol, 50 μL of 105 mM EDC (Sigma Aldrich, USA) in methanol and 50 μL of 2.5% pyridine (Sigma Aldrich, USA) in methanol[46]. After reaction at 4 °C for 30 min, the mixtures were evaporated to dryness and re-dissolved in 50 μL of 50% methanol for the UHPLC-HRMS assay[51]. The chromatographic separation was performed on a Thermo Fisher Ultimate 3000 UHPLC system using a Waters HSS T3 column (2.1 mm × 100 mm, 1.7 μm) (Waters, USA). The mobile phases comprised water with 0.1% formate (phase A) and acetonitrile with 0.1% formate (phase B). Metabolites were separated by linear gradient mode (0–0.5 min, 5% B; 2.5 min, 30% B; 5.5 min, 60% B; 9–13 min, 100% B; 13.1–15 min, 5% B) and mass spectrometry data were collected using Thermo Fisher Q Exactive Hybrid Quadrupole-Orbitrap Mass Spectrometry (QE) in Heated Electrospray Ionization Negative (HESI-) mode. The spray voltage was set to 2800 V. The capillary and probe heater temperatures were adjusted to 320 °C and 350 °C, respectively. The sheath gas flow rate was 50 Arb (arbitrary unit), the auxiliary gas flow rate was tuned to 15 Arb, and the S-Lens RF level was 50 Arb. The full scan was operated at a high-resolution 7×10^4 FWHM (m/z, 200) at 100–1000 m/z with an AGC target setting of 1×10^6. Data were analyzed using Xcalibur software, and IsoCor v2 was used to correct the original mass spectra[51].

Reporting summary

Further information on research design is available in the Nature Portfolio Reporting Summary linked to this article.

Data availability

Numerical data were plotted using GraphPad Prism 8 (GraphPad Software Inc., USA). Statistical analysis was performed using the Student's *t* test, two-way ANOVA and log-rank Mantel–Cox test. The genome sequencing data are deposited and released with the accession numbers PRJNA1108415, PRJNA1109294 and PRJNA1108442. Transcriptomics sequencing data are available in the short read archive (SRA) of the National Center for Biotechnology Information database (accession number PRJNA943448). Reference genome of the *Toxoplasma* GT1 strain: https://toxodb.org/toxo/app/record/dataset/NCBITAXON_507601. All data are presented in the article or the supplementary information. The source data for the graphs and images can be found in the Supplementary Data 4. All resources described herein are available upon reasonable request.

Received: 6 August 2024; Accepted: 26 February 2025;
Published online: 07 March 2025

References

1. Dubey, J. P. *Toxoplasmosis of Animals and Humans*, 3rd edn., 564 (Toxoplasmosis of Animals and Humans, 2021).
2. Dunay, I. R. et al. Treatment of toxoplasmosis: historical perspective, animal models, and current clinical practice. *Clin. Microbiol. Rev.* **31**, https://doi.org/10.1128/cmr.00057-17 (2018).
3. Azadi, Y., Ahmadpour, E. & Ahmadi, A. Targeting strategies in therapeutic applications of Toxoplasmosis: recent advances in liposomal vaccine delivery systems. *Curr. Drug Targets* **21**, 541–558 (2020).
4. Montazeri, M. et al. Drug resistance in *Toxoplasma gondii*. *Front. Microbiol.* **9**, 2587 (2018).
5. Hiszczyńska-Sawicka, E., Gatkowska, J. M., Grzybowski, M. M. & Długońska, H. Veterinary vaccines against toxoplasmosis. *Parasitology* **141**, 1365–1378 (2014).
6. Wang, J.-L. et al. Advances in the development of anti-*Toxoplasma gondii* vaccines: challenges, opportunities, and perspectives. *Trends Parasitol.* **35**, 239–253 (2019).
7. Blume, M. et al. Host-derived glucose and its transporter in the obligate intracellular pathogen *Toxoplasma gondii* are dispensable by glutaminolysis. *Proc. Natl Acad. Sci. USA* **106**, https://doi.org/10.1073/pnas.0903831106 (2009).
8. MacRae, J. I. et al. Mitochondrial metabolism of glucose and glutamine is required for intracellular growth of *Toxoplasma gondii*. *Cell Host Microbe* **12**, 682–692 (2012).
9. Blume, M. et al. A *Toxoplasma gondii* gluconeogenic enzyme contributes to robust central carbon metabolism and is essential for replication and virulence. *Cell Host Microbe* **18**, 210–220 (2015).
10. Nitzsche, R., Zagoriy, V., Lucius, R. & Gupta, N. Metabolic cooperation of glucose and glutamine is essential for the lytic cycle of obligate intracellular parasite *Toxoplasma gondii*. *J. Biol. Chem.* **291**, 126–141 (2016).
11. Nitzsche, R. et al. A plant/fungal-type phosphoenolpyruvate carboxykinase located in the parasite mitochondrion ensures glucose-independent survival of *Toxoplasma gondii*. *J. Biol. Chem.* **292**, 15225–15239 (2017).

12. Ningbo, X. et al. Pyruvate homeostasis as a determinant of parasite growth and metabolic plasticity in *Toxoplasma gondii*. *mBio* **10**, https://doi.org/10.1128/mBio.00898-19 (2019).
13. Lyu, C. et al. The mitochondrial pyruvate carrier coupling glycolysis and the tricarboxylic acid cycle is required for the asexual reproduction of *Toxoplasma gondii*. *Microbiol. Spectr.* **11**, e05043–05022 (2023).
14. Oppenheim, R. D. et al. BCKDH: the missing link in apicomplexan mitochondrial metabolism is required for full virulence of *Toxoplasma gondii* and *Plasmodium berghei*. *PLoS Pathog.* **10**, e1004263 (2014).
15. Fleige, T., Pfaff, N., Gross, U. & Bohne, W. Localisation of gluconeogenesis and tricarboxylic acid (TCA)-cycle enzymes and first functional analysis of the TCA cycle in *Toxoplasma gondii*. *Int. J. Parasitol.* **38**, 1121–1132 (2008).
16. Lykins, J. et al. From *Tg*O/GABA-AT, GABA, and T-263 mutant to conception of *Toxoplasma*. *iScience* **27**, 108477 (2023).
17. Krishnan, A. et al. Functional and computational genomics reveal unprecedented flexibility in stage-specific *Toxoplasma* metabolism. *Cell Host Microbe* **27**, 290–306 (2020).
18. Sidik, S. M. et al. A Genome-wide CRISPR screen in *Toxoplasma* identifies essential apicomplexan genes. *Cell* **166**, 1423–1435, (2016).
19. Silva, M. F. et al. Functional and biochemical characterization of the *Toxoplasma gondii* succinate dehydrogenase complex. *PLoS Pathog.* **19**, e1011867 (2023).
20. Ait-El-Mkadem, S. et al. Mutations in MDH2, encoding a krebs cycle enzyme, cause early-onset severe encephalopathy. *Am. J. Hum. Genet.* **100**, 151–159 (2017).
21. Mocholi, E. et al. Pyruvate metabolism controls chromatin remodeling during CD4(+) T cell activation. *Cell Rep.* **42**, https://doi.org/10.1016/j.celrep.2023.112583 (2023).
22. Liu, X. et al. The existence of a nonclassical TCA cycle in the nucleus that wires the metabolic-epigenetic circuitry. *Sig. Transduct. Targeted Therapy* **6**, https://doi.org/10.1038/s41392-021-00774-2 (2021).
23. Lyu, C. et al. Two enzymes contribute to citrate production in the mitochondrion of *Toxoplasma gondii*. *J. Biol. Chem.* **300**, 107565 (2024).
24. Pino, P. et al. Dual targeting of antioxidant and metabolic enzymes to the mitochondrion and the apicoplast of *Toxoplasma gondii*. *PLoS Pathog.* **3**, e115 (2007).
25. Limenitakis, J. et al. The 2-methylcitrate cycle is implicated in the detoxification of propionate in *Toxoplasma gondii*. *Mol. Microbiol.* **87**, 894–908 (2013).
26. Niikura, M. et al. Suppression of experimental cerebral malaria by disruption of malate:quinone oxidoreductase. *Malar. J.* **16**, 247 (2017).
27. Qian, J. et al. Mitochondrial ADP/ATP carrier 1 is important for the growth of *Toxoplasma* tachyzoites. *Microbiol. Spectr.* **11**, e00040–00023 (2023).
28. Wu, Y. et al. Depletion of *Toxoplasma* adenine nucleotide translocator leads to defects in mitochondrial morphology. *Parasites Vectors* **15**, https://doi.org/10.1186/s13071-022-05295-7 (2022).
29. Cui, J. et al. A coccidia-specific phosphate transporter is essential for the growth of *Toxoplasma gondii* parasites. *Microbiol. Spectr.* **10**, e02186–02122 (2022).
30. Barylyuk, K. et al. A comprehensive subcellular atlas of the *Toxoplasma* Proteome *via* hyperLOPIT provides spatial context for protein functions. *Cell Host Microbe* **28**, 752–766 (2020).
31. Ningbo, X. et al. Metabolic flexibilities and vulnerabilities in the pentose phosphate pathway of the zoonotic pathogen *Toxoplasma gondii*. *PLoS Pathog.* **18**, e1010864 (2022).
32. Chen, L. et al. NADPH production by the oxidative pentose-phosphate pathway supports folate metabolism. *Nat. Metab.* **1**, 404–415 (2019).
33. Pek, J. W., Anand, A. & Kai, T. Tudor domain proteins in development. *Development* **139**, 2255–2266 (2012).
34. Hossain, M. J. et al. Tudor domain proteins in protozoan parasites and characterization of *Plasmodium falciparum* tudor staphylococcal nuclease. *Int. J. Parasitol.* **38**, 513–526 (2008).
35. Manage, K. I. et al. A tudor domain protein, SIMR-1, promotes siRNA production at piRNA-targeted mRNAs in C. elegans. *eLife* **9**, e56731 (2020).
36. Wiese, M. & Bannister, A. J. Two genomes, one cell: Mitochondrial-nuclear coordination *via* epigenetic pathways. *Mol. Metabol.* **38**, https://doi.org/10.1016/j.molmet.2020.01.006 (2020).
37. Shao, Z. et al. Nuclear pyruvate dehydrogenase complex regulates histone acetylation and transcriptional regulation in the ethylene response. *Science advances.* **10**, eado2825 (2024).
38. Huynh, M.-H. & Carruthers, V. B. Tagging of endogenous genes in a *Toxoplasma gondii* strain lacking Ku80. *Eukaryotic Cell* **8**, https://doi.org/10.1128/ec.00358-08 (2009).
39. Hunt, A. et al. Differential requirements for cyclase-associated protein (CAP) in actin-dependent processes of *Toxoplasma gondii*. *eLife* **8**, e50598 (2019).
40. Andenmatten, N. et al. Conditional genome engineering in *Toxoplasma gondii* uncovers alternative invasion mechanisms. *Nat. Methods* **10**, 125–127 (2013).
41. Brown, K. M., Long, S. & Sibley, L. D. Plasma membrane association by N-acylation governs PKG function in *Toxoplasma gondii*. *mBio* **8**, https://doi.org/10.1128/mBio.00375-17 (2017).
42. Qureshi, B. M. et al. Dynein light chain 8a of *Toxoplasma gondii*, a unique conoid-localized β-strand-swapped homodimer, is required for an efficient parasite growth. *FASEB J.* **27**, 1034–1047 (2013).
43. Günay-Esiyok, Ö., Scheib, U., Noll, M. & Gupta, N. An unusual and vital protein with guanylate cyclase and P4-ATPase domains in a pathogenic protist. *Life Sci. Alliance* **2**, https://doi.org/10.26508/lsa.201900402 (2019).
44. Li, C.-G. et al. Evodiamine Augments NLRP3 Inflammasome Activation and Anti-bacterial Responses Through Inducing α-Tubulin Acetylation. *Front. Pharmacol.* **10**, https://doi.org/10.3389/fphar.2019.00290 (2019).
45. Wu, M. et al. Live-attenuated ME49*Δcdpk3* strain of *Toxoplasma gondii* protects against acute and chronic toxoplasmosis. *npj Vaccines* **7**, 98 (2022).
46. Ningbo, X. et al. Functional analysis of *Toxoplasma* lactate dehydrogenases suggests critical roles of lactate fermentation for parasite growth *in vivo*. *Cell. Microbiol.* **20**, e12794 (2018).
47. Ningbo, X. et al. A Lactate Fermentation Mutant of *Toxoplasma* Stimulates Protective Immunity Against Acute and Chronic Toxoplasmosis. *Front. Immunol.* **9**, https://doi.org/10.3389/fimmu.2018.01814 (2018).
48. Yang, J. et al. ANK1 and DnaK-TPR, two tetratricopeptide repeat-containing proteins primarily expressed in *Toxoplasma* bradyzoites, do not contribute to bradyzoite differentiation. *Front. Microbiol.* **8**, 2210 (2017).
49. Cui, J. & Shen, B. Transcriptomic analyses reveal distinct response of porcine macrophages to *Toxoplasma gondii* infection. *Parasitol. Res.* **119**, 1819–1828 (2020).
50. Millard, P. et al. IsoCor: isotope correction for high-resolution MS labeling experiments. *Bioinformatics* **35**, 4484–4487 (2019).
51. Rende, U., Niittylä, T. & Moritz, T. Two-step derivatization for determination of sugar phosphates in plants by combined reversed phase chromatography/tandem mass spectrometry. *Plant Methods* **15**, 127 (2019).

Acknowledgements

We thank Na Li, Yaqiong Guo, Dongjuan Yuan and Rui Xu (College of Veterinary Medicine, South China Agricultural University, Guangzhou) for the discussion. We thank Xianfu Gao (Shanghai Profleader Biotech Co., Ltd.) and Wenchao Wang (Phenions Biotech Co., Ltd.) for LC-MS/MS. The

authors also thank the Institute of Hematology, Jinan University, for providing flow cytometric sorting. This research was supported by the National Key Research and Development Program of China (2023YFD1801000); Guangdong Major Project of Basic and Applied Basic Research (2020B0301030007); National Key Research and Development Program of China (2022YFD1800200; 2022YFD1801700); Natural Science Foundation of Guangdong Province (2022A1515011104; 2024A1515011346); 111 Project (D20008); Double first-class discipline promotion project (2023B10564003). Supplementary funding was provided *via* a Core Research Grant to Nishith Gupta (CRG/2021/000919) by the Department of Science and Technology – Science and Engineering Research Board (DST-SERB), India. Nishith Gupta also acknowledges the extended support of the Senior fellowship by the DBT–Wellcome Trust (India Alliance, IA/S/19/1/504263) and the Scholar Mobility Program from the Sino-German Science Center (M0074). The funders had no role in the design, data collection, analysis, preparation or decision to publish this work.

Author contributions

Hongxi Zhang: Resources; Data curation; Validation; Investigation; Methodology; Writing–original draft. Nuo Ji: Resources; Data curation; Validation; Investigation; Methodology; Writing–original draft. Shuxin Su: Resources; Data curation; Validation; Investigation; Methodology; Writing–original draft. Meng Zhao: Resources; Data curation; Validation; Investigation; Methodology. Huiyu Du: Resources; Data curation; Validation; Investigation; Methodology. Lakesh Kumar Sahoo: Resources; Validation; Investigation; Methodology. Yi Wu: Resources; Data curation; Validation; Investigation; Methodology; Supervision; Writing–original draft. Yaoyu Feng: Resources; Data curation; Formal analysis; Supervision; Funding acquisition; Project administration; Nishith Gupta: Resources; Data curation; Supervision; Funding acquisition; Project administration; Writing—review and editing. Lihua Xiao: Resources; Data curation; Formal analysis; Supervision; Funding acquisition; Project administration; Ningbo Xia: Conceptualization; Resources; Data curation; Software; Formal analysis; Validation; Investigation; Visualization; Methodology; Supervision; Funding acquisition; Project administration; Writing—original draft; Writing—review and editing.

Competing interests

The authors declare that they have no conflict of interest. N.G. is an Editorial Board Member for Communications Biology, but was not involved in the editorial review of, nor the decision to publish this article.

Additional information

Supplementary information The online version contains supplementary material available at https://doi.org/10.1038/s42003-025-07823-4.

Correspondence and requests for materials should be addressed to Nishith Gupta, Lihua Xiao or Ningbo Xia.

Peer review information *Communications Biology* thanks the anonymous reviewers for their contribution to the peer review of this work. Primary Handling Editors: Karthika Rajeeve and Dario Ummarino.

Reprints and permissions information is available at http://www.nature.com/reprints

Publisher's note Springer Nature remains neutral with regard to jurisdictional claims in published maps and institutional affiliations.

Open Access This article is licensed under a Creative Commons Attribution-NonCommercial-NoDerivatives 4.0 International License, which permits any non-commercial use, sharing, distribution and reproduction in any medium or format, as long as you give appropriate credit to the original author(s) and the source, provide a link to the Creative Commons licence, and indicate if you modified the licensed material. You do not have permission under this licence to share adapted material derived from this article or parts of it. The images or other third party material in this article are included in the article's Creative Commons licence, unless indicated otherwise in a credit line to the material. If material is not included in the article's Creative Commons licence and your intended use is not permitted by statutory regulation or exceeds the permitted use, you will need to obtain permission directly from the copyright holder. To view a copy of this licence, visit http://creativecommons.org/licenses/by-nc-nd/4.0/.

© The Author(s) 2025